

# CrystEngComm

Accepted Manuscript



This is an *Accepted Manuscript*, which has been through the Royal Society of Chemistry peer review process and has been accepted for publication.

*Accepted Manuscripts* are published online shortly after acceptance, before technical editing, formatting and proof reading. Using this free service, authors can make their results available to the community, in citable form, before we publish the edited article. We will replace this *Accepted Manuscript* with the edited and formatted *Advance Article* as soon as it is available.

You can find more information about *Accepted Manuscripts* in the [Information for Authors](#).

Please note that technical editing may introduce minor changes to the text and/or graphics, which may alter content. The journal's standard [Terms & Conditions](#) and the [Ethical guidelines](#) still apply. In no event shall the Royal Society of Chemistry be held responsible for any errors or omissions in this *Accepted Manuscript* or any consequences arising from the use of any information it contains.

# Coordination Polymers Based on a Glycine-Derivative Ligand

Sérgio M. F. Vilela,<sup>a,b</sup> Duarte Ananias,<sup>a</sup> Patrícia Silva,<sup>a</sup> Mariela Nolasco,<sup>a</sup>  
Luís D. Carlos,<sup>c</sup> Verónica de Zea Bermudez,<sup>d</sup> João Rocha,<sup>a</sup>  
João P. C. Tomé,<sup>b</sup> Filipe A. Almeida Paz<sup>a,\*</sup>

*A contribution from*

<sup>a</sup> *Department of Chemistry, CICECO, University of Aveiro, 3810-193 Aveiro, Portugal*

<sup>b</sup> *Department of Chemistry, QOPNA, University of Aveiro, 3810-193 Aveiro, Portugal*

<sup>c</sup> *Department of Physics, CICECO, University of Aveiro, 3810-193 Aveiro, Portugal*

<sup>d</sup> *Department of Chemistry, CQ-VR, University of Trás-os-Montes e Alto Douro, 5001-801  
Vila Real, Portugal*

---

*To whom correspondence should be addressed:*

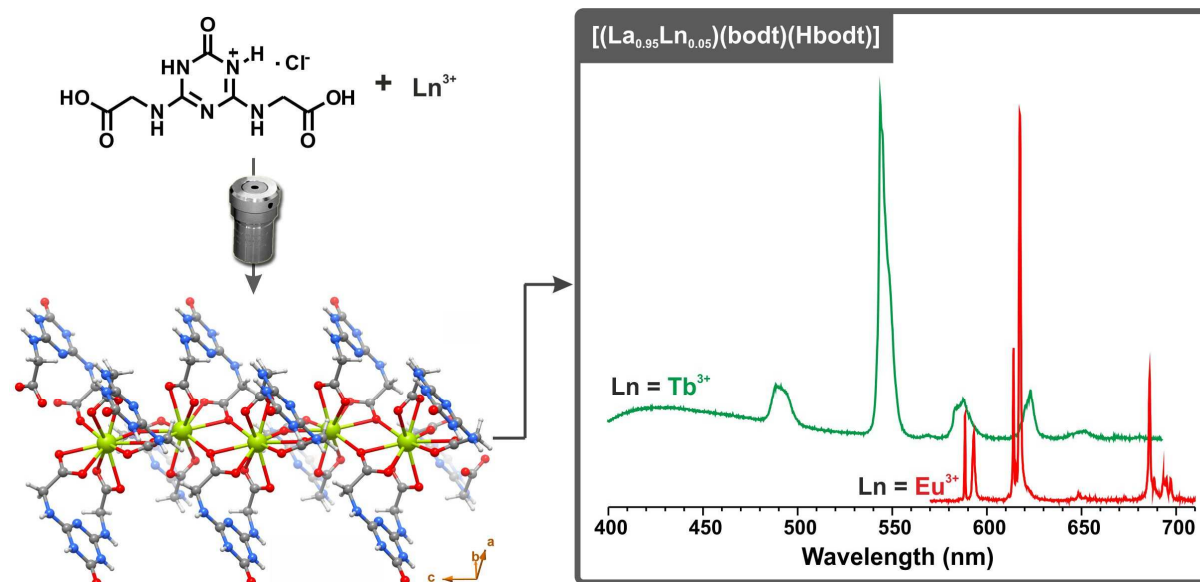
Filipe A. Almeida Paz  
Department of Chemistry, CICECO  
University of Aveiro  
3810-193 Aveiro  
Portugal

E-mail: [filipe.paz@ua.pt](mailto:filipe.paz@ua.pt)  
FAX: (+351) 234 401470  
Telephone: (+351) 234 370200 (Ext. 23553)

## Abstract

The combination between the glycine-derivative supramolecular salt 4,6-bis(carboxymethylamino)-2-oxo-2,3-dihydro-1,3,5-triazin-1-ium chloride ( $\text{H}_2\text{bodt}\cdot\text{HCl}$ ) with lanthanide(III) chloride hydrates under hydrothermal conditions (120 °C, 48 h), led to the formation of a family of isotypical materials formulated as  $[\text{Ln}(\text{bodt})(\text{Hbodt})]$  [where  $\text{Ln}^{3+} = \text{La}^{3+}$  (**1**),  $(\text{La}_{0.95}\text{Eu}_{0.05})^{3+}$  (**2**) and  $(\text{La}_{0.95}\text{Tb}_{0.05})^{3+}$  (**3**)]. The synthesis of the novel precursor  $\text{H}_2\text{bodt}\cdot\text{HCl}$  is detailed. The structures of  $\text{H}_2\text{bodt}\cdot\text{HCl}$  and its intermediated compound were unveiled by single-crystal X-ray diffraction and characterized by standard liquid-state techniques. The crystallographic details of compound **1** were unveiled in the monoclinic  $P2_1/c$  space group by using single-crystal X-ray diffraction, with the crystal structure of **1** comprising an one-dimensional  $\infty^1[\text{La}(\text{bodt})(\text{Hbodt})]$  coordination polymer. All polymeric materials were fully characterized by FT-IR, electron microscopy (SEM and EDS), powder X-ray diffraction, elemental and thermogravimetric analysis. The photoluminescent properties of **1** and of the mixed-lanthanide materials **2** and **3** were investigated at ambient and low temperatures. An excited-state intermolecular proton transfer (ESPT) process, induced by intermolecular hydrogen-bonding interactions, is proposed to account for the observed anomalous emission and excitation spectra of **1**. Aiming at providing an in-depth understanding of the emission (fluorescence and phosphorescence) properties of the ligand, time-dependent density functional theory (TD-DFT) calculations were also performed.

## Graphical abstract



# 1. Introduction

Multidimensional Coordination Polymers (CPs), also known as Metal-Organic Frameworks (MOFs), are a class of crystalline and ordered compounds that have attracted the attention of worldwide researchers working in various fields of science, spanning from crystal engineering and supramolecular chemistry to materials chemistry and physics.<sup>1</sup> Taking advantage of their hybrid nature (*i.e.*, the simultaneous presence of inorganic and organic components) CPs have shown great potentiality to be applied in a wide range of areas such as in heterogeneous catalysis,<sup>2</sup> in gas storage and separations,<sup>3</sup> for the capture of CO<sub>2</sub>,<sup>3a, 4</sup> in magnetic materials,<sup>5</sup> as ion-exchangers,<sup>6</sup> as optical sensors<sup>7</sup> or photoluminescent materials,<sup>8</sup> among several others.

The organic primary building unity (PBU) displays a key importance in the design and preparation of the CPs due to its enormous flexibility: linkers may be aromatic or aliphatic, rigid or flexible and may have different functional coordinating groups (*e.g.*, carboxylates, phosphonates, sulphonates, imidazoles, triazoles, tetrazoles and pyridyl groups). Naturally-occurring amino acids are biomolecules having in their structure at least two functional coordinating groups (an amino and a carboxylic acid groups) which permit themselves the existence of various types of coordination modes and supramolecular interactions (*e.g.*, hydrogen bonds) with other interacting sites/groups.<sup>9</sup> This structural feature, availability, cost and the bio-compatibility of these molecules make them highly attractive organic PBUs for the preparation of multidimensional CPs, yielding the so-called bio-CPs (BCPs).<sup>10</sup> Additionally, due to their chirality (with the exception of glycine), amino acids and their derivatives are attractive organic PBUs to induce chirality into the final BCPs architectures.<sup>10a, 11</sup> Interesting examples of CPs containing, as for instance, aspartic acid,<sup>12</sup> glycine,<sup>13</sup> proline,<sup>13-14</sup> cysteine,<sup>10b</sup> tryptophan,<sup>15</sup> glutamine,<sup>16</sup> methionine<sup>9b</sup> and histidine<sup>17</sup> have been described in the literature. Remarkably, the use of pure natural amino acids as organic PBUs typically leads to mostly 1D CPs,<sup>12b, 12e, 15, 18</sup> with lamellar and framework extended structures being significantly more scarce.<sup>11, 19</sup> The design of 3D structures is typically achieved using other organic ligands (co-ligand) together with the amino acids as, for instance, 1,3,5-benzenetricarboxylic acid,<sup>17a</sup> 4,4'-bipyridine,<sup>12c, 14-15, 20</sup> 4,4'-azopyridine, bis(4-pyridyl)ethylene, 1,4-bis(4-pyridyl)benzene, tris(4-pyridyl)triazine and 3,5-bis(4-pyridyl)pyridine.<sup>21</sup> Taking advantage of the reactivity of the amino group while keeping the carboxylic group unaltered, the structures of these organic PBUs are very often modified. Researchers have, for example, prepared organic molecules with more coordinating groups while maintaining the same ligand backbone: i) a carboxylic acid group and a pyridyl in leucine, serine, valine and threonine;<sup>11, 22</sup> ii) a carboxylic acid group and a phenylcarboxylate in serine and valine;<sup>23</sup> iii) a carboxylic acid group and a tetrazole in phenylalanine and glycine.<sup>24</sup>

Glycine is the simplest amino acid and has a very flexible structure. When compared with rigid ligands, flexible molecules afford less predictable materials, although they are usually unprecedented and interesting due to the high conformational freedom of the linkers. To minimize this limitation, Bai's

group have reported a glycine-based derivative,  $N,N',N''$ -1,3,5-triazine-2,4,6-triyltrisglycine ( $H_3TTG$ ), containing a central aromatic triazine ring which confers higher rigidity to the resulting organic PBU.<sup>25</sup>  $H_3TTG$  is an attractive organic ligand for the synthesis of multidimensional CPs, because: i) it has multiple coordination sites providing the possibility to prepare architectures with high dimensionality; ii) it still possesses a high level of flexibility due to the presence of  $-NHCH_2-$  moieties; iii) the presence of several O and N atoms and the aromatic ring may form hydrogen bonds and  $\pi$ - $\pi$  stacking interactions; and iv) depending of the deprotonation level, the carboxylate group may adopt various coordination modes. The self-assembly between  $H_3TTG$  and  $Ni^{2+}$ ,  $Co^{2+}$  and  $Cd^{2+}$  as metal centers originated functional 2D and 3D CPs with interesting magnetic, luminescent and adsorption properties.<sup>25a, 25c, 25d</sup>

Following our interest in the design and preparation of functional CPs,<sup>26</sup> and based on the design principles of the research group of Bai,<sup>25</sup> in this manuscript we report, in a first stage, the optimized reaction to successfully prepare the glycine-derivative supramolecular salt 4,6-bis(carboxymethylamino)-2-oxo-2,3-dihydro-1,3,5-triazin-1-ium chloride ( $H_2bodt \cdot HCl$ ), isolated in quantitative yields; in a second stage, this product was used as an organic PBU to react with lanthanide(III) chloride hydrates to prepare a novel family of isotypical materials formulated as  $[Ln(bodt)(Hbodt)]$  [where  $Ln^{3+} = La^{3+}$  (**1**),  $(La_{0.95}Eu_{0.05})^{3+}$  (**2**) and  $(La_{0.95}Tb_{0.05})^{3+}$  (**3**)], under typical static hydrothermal conditions. All materials, and intermediate molecules for the preparation of the ligand precursor  $H_2bodt \cdot HCl$ , have been extensively characterized both in the liquid and in the solid state. X-ray diffraction studies revealed that compound **1**, and the remaining members of the series, is formed by a one-dimensional  $\infty^1[La(bodt)(Hbodt)]$  coordination polymer which is interconnected in the crystal structure by cooperative  $N-H \cdots (N,O)$  hydrogen bonds to yield a complex framework-type structure. Proper characterization of hydrogen bonding sub-networks within CPs is typically very difficult unless a detailed theoretical vibrational study can be performed *in silico*.<sup>27</sup> In this manuscript we further show that photoluminescence spectroscopy can provide additional information route for the presence of typical hydrogen bonding synthons. Indeed, sharp bands were observed in the excitation and emission spectra of the glycine-derivative CPs herein reported which could only be explained by complementing the photoluminescence spectroscopy experiments with quantum chemical calculations. Indeed, methods based on density functional theory (DFT) together with its time-dependent formalism (TD-DFT) have been shown to produce reliable results when applied to lanthanide complexes.<sup>28</sup> We have used a similar approach to study the observed properties for the  $[Ln(bodt)(Hbodt)]$  system, which allowed us to determine the changes in the structural and electronic properties, with special emphasis in the excitation energies, molecular orbital compositions and triplet and singlet excited state energies, ultimately allowing a theoretical rationalization of the experimental photophysical results.

## 2. Experimental section

### 2.1. General Instrumentation

SEM (Scanning Electron Microscopy) images were collected using either a Hitachi S-4100 field emission gun tungsten filament instrument working at 25 kV, or a high-resolution Hitachi SU-70 working at 4 kV. Samples were prepared by deposition on aluminium sample holders followed by carbon coating using an Emitech K950X carbon evaporator. EDS (Energy Dispersive X-ray Spectroscopy) data and SEM mapping images were recorded using the latter microscope working at 15 kV and using a Bruker Quantax 400 or a Sprit 1.9 EDS microanalysis system.

Thermogravimetric analyses (TGA) were performed on a Shimadzu TGA 50 equipment, from ambient temperature to 650 °C, with a heating rate of 5 °C min<sup>-1</sup> under a continuous nitrogen atmosphere with a flow rate of 20 mL min<sup>-1</sup>.

Fourier-Transform Infrared (FT-IR) spectra in the 3500-450 cm<sup>-1</sup> range were recorded as KBr pellets (FT-IR spectroscopy grade, BDH SpectroSol) using a Mattson 7000 FT-IR spectrometer by averaging 200 scans at a maximum resolution of 2 cm<sup>-1</sup>. Typically, 2 mg of the sample were mixed in a mortar with 200 mg of KBr to produce the pellets.

Elemental analyses for carbon, hydrogen and nitrogen were performed with a LECO CHNS - 932 elemental analyzer at the Department of Chemistry, University of Aveiro. Typical samples (between 1 and 2 mg) were combusted at 1000 °C for 4 minutes under an oxygen atmosphere. Helium was used as the carrier gas.

Routine Powder X-Ray Diffraction (PXRD) data for all materials were collected at ambient temperature on an X'Pert MPD Philips diffractometer (Cu K<sub>α1,2</sub>X-radiation, λ<sub>1</sub> = 1.540598 Å; λ<sub>2</sub> = 1.544426 Å), equipped with an X'Celerator detector and a flat-plate sample holder in a Bragg-Brentano para-focusing optics configuration (40 kV, 50 mA). Intensity data were collected by the step-counting method (step 0.04°), in continuous mode, in the *ca.* 5 ≤ 2θ ≤ 50° range.

<sup>1</sup>H and <sup>13</sup>C solution NMR spectra were recorded on a Bruker Avance 300 spectrometer at 300.13 and 75.47 MHz, respectively. Deuterated chloroform (CDCl<sub>3</sub>) and dimethylsulfoxide-*d*<sub>6</sub> (DMSO-*d*<sub>6</sub>) were used as solvents and tetramethylsilane as internal reference. Chemical shifts (δ) are expressed in ppm and the coupling constants (*J*) in Hz.

Mass spectra were recorded with a Micromass Q-TOF2 equipment. Dichloromethane was used as solvent for 2-chloro-4,6-bis(methoxycarbonylmethylamine)-1,3,5-triazine (**L'**) and water for 4,6-bis(carboxymethylamino)-2-oxo-dihydro-1,3,5-triazinium chloride (H<sub>2</sub>bodt·HCl). The employed concentration was 1 mg/mL. Samples were diluted in methanol to a concentration of 2 μL (sample)/200 μL (methanol).

## 2.2 - Chemicals

Chemicals were readily available from commercial sources and were used as received without further purification: cyanuric chloride ( $C_3Cl_3N_3$ , 99%, Sigma-Aldrich); glycine methyl ester hydrochloride ( $H_2NCH_2CO_2CH_3 \cdot HCl$ , 99%, Sigma-Aldrich); potassium carbonate ( $K_2CO_3$ , 99%, Panreac); lanthanide(III) chloride hydrates ( $LaCl_3 \cdot 7H_2O$ ,  $EuCl_3 \cdot 6H_2O$ ,  $TbCl_3 \cdot 6H_2O$ , 99.9%, Sigma-Aldrich); acetone ( $C_3H_6O$ , pure, Sigma-Aldrich); dichloromethane ( $CH_2Cl_2$ , pure, Sigma-Aldrich); methanol ( $CH_3OH$ , pure, Sigma-Aldrich); hydrochloric acid (HCl, 37%, Panreac); chloroform-*d* ( $CDCl_3$ , 99.8%, CIL - Cambridge Isotope Laboratories, Inc.); dimethylsulfoxide-*d*<sub>6</sub> (DMSO-*d*<sub>6</sub>, 99%, CIL - Cambridge Isotope Laboratories, Inc.).

## 2.3. Synthesis of 4,6-bis(carboxymethylamino)-2-oxo-2,3-dihydro-1,3,5-triazin-1-ium chloride ( $H_2bodt \cdot HCl$ )

Cyanuric chloride (100 mg, 0.54 mmol) was added to a mixture of glycine methyl ester hydrochloride (106 mg, 1.19 mmol, 2.2 eq.) and potassium carbonate (150 mg, 1.09 mmol) in acetone (5 mL) at 0 °C. The reaction mixture was kept under magnetic stirring at ambient temperature for approximately 24 h under anhydrous atmosphere. The solvent was afterwards distilled under reduced pressure, and a liquid/liquid extraction was performed using a mixture of dichloromethane and water (5:1). The final product, 2-chloro-4,6-bis(methoxycarbonylmethylamine)-1,3,5-triazine (*L'*), was obtained by recrystallization from a mixture of dichloromethane and methanol (3:1) in 62% yield.

*L'* (50 mg, 0.17 mmol) was treated with an aqueous solution of HCl 6M (5 mL) under reflux for 3 h, with continuous magnetic stirring. The reaction product was washed with dichloromethane and the aqueous phase was distilled under reduced pressure. The desired organic ligand, 4,6-bis(carboxymethylamino)-2-oxo-2,3-dihydro-1,3,5-triazin-1-ium chloride ( $H_2bodt \cdot HCl$ ), was obtained in quantitative yields.

***L'***:  $^1H$  NMR (300.13 MHz,  $CDCl_3$ )  $\delta$ : 3.79 (s, 6H,  $CH_3$ ), 4.15 (d, 4H,  $J = 6.0$  Hz,  $CH_2$ ) and 5.74-5.93 (m, 2H, NH);

$^{13}C$  NMR (75.47 MHz,  $CDCl_3/DMSO-d_6$ )  $\delta$ : 41.8 ( $\underline{CH_2}$ ), 51.4 ( $\underline{CH_3}$ ), 165.4 ( $\underline{CNH}$ ), 168.0 ( $\underline{CCI}$ ) and 169.7 ( $\underline{CO_2Me}$ );

MS (TOF MS ES<sup>+</sup>)  $m/z$ : 290.1 (M+H)<sup>+</sup>.

**$H_2bodt \cdot HCl$** :  $^1H$  NMR (300.13 MHz, DMSO-*d*<sub>6</sub>)  $\delta$ : 4.10 (d, 4H,  $J = 5.75$  Hz,  $CH_2$ ) and 8.57 (t, 2H,  $J = 5.75$  Hz, NH);

$^{13}C$  NMR (75.47 MHz, DMSO-*d*<sub>6</sub>)  $\delta$ : 42.6 ( $\underline{CH_2}$ ), 146.8 (NH- $\underline{C=O}$ ), 156.7 ( $\underline{C=N}$ ) and 169.6 ( $\underline{CO_2H}$ );

MS (TOF MS ES<sup>+</sup>)  $m/z$ : 244.1 (M)<sup>+</sup>.

## 2.4. Hydrothermal Synthesis of [La(bodt)(Hbodt)]

A reactive mixture composed of 0.0467 g of H<sub>2</sub>bodt·HCl and 0.062 g of LaCl<sub>3</sub>·7H<sub>2</sub>O in distilled water (*ca.* 6 mL) was prepared at ambient temperature having an overall molar ratio of approximately 1 : 1 : 2000 (H<sub>2</sub>bodt·HCl : La<sup>3+</sup> : H<sub>2</sub>O). The mixture was kept under constant magnetic stirring for approximately 30 min. The resulting homogenous suspension was then transferred to a Teflon-lined Parr Instrument autoclave and placed inside a MMM Venticell oven where remained at 120 °C for 48 h. After reacting the oven was turned off and the vessels were allowed to slowly cool to ambient temperature while inside the oven. The resulting material [La(bodt)(Hbodt)] (**1**) was recovered by vacuum filtration, washed with copious amounts of distilled water and air dried at ambient temperature.

The isotypical materials with 5% of Eu<sup>3+</sup> (**2**) and Tb<sup>3+</sup> (**3**) were prepared as described above for compound **1** while adjusting the amounts of the lanthanide chloride salts in the initial reactive mixture to the desired percentages.

Thermogravimetric analysis (TGA) data (weight losses in %) and derivative thermogravimetric peaks (DTG; in italics inside the parentheses).

**1**: 269-424 °C -28.5% (*405 °C*); 424-593 °C -39.3% (*450 °C*).

**2**: 284-425 °C -31.5% (*408 °C*); 425-600 °C -39.4% (*452 °C*).

**3**: 275-426 °C -29.3% (*408 °C*); 426-597 °C -40.9% (*454 °C*).

Elemental CH composition (%).

Calcd for **1**: C 27.02; H 2.43; N 22.51. Found: C 26.72; H 2.61; N 22.98.

Calcd for **2**: C 26.99; H 2.43; N 22.49. Found: C 26.30; H 2.68; N 22.54.

Calcd for **3**: C 26.98; H 2.43; N 22.48. Found: C 26.98; H 2.74; N 23.06.

Selected FT-IR data (in cm<sup>-1</sup>; KBr pellets).

**1**: ν(N-H) = 3334*m*; ν(-CH<sub>2</sub>-) = 2992*w*; ν(C=O) = 1752*w*; ν(-CO<sub>2</sub><sup>-</sup>) = 1571*vs*; ν<sub>asym</sub>(-CO<sub>2</sub><sup>-</sup>) = 1517*s*; ν<sub>sym</sub>(-CO<sub>2</sub><sup>-</sup>) = 1431*s*; ν(=C-N) = 1360-1200*m-s*; ν(C-N) = 1173*w* and 1144*w*; δ(N-H) = 738*m*.

**2**: ν(N-H) = 3334*m*; ν(-CH<sub>2</sub>-) = 2994*w*; ν(C=O) = 1752*w*; ν(-CO<sub>2</sub><sup>-</sup>) = 1571*vs*; ν<sub>asym</sub>(-CO<sub>2</sub><sup>-</sup>) = 1518*s*; ν<sub>sym</sub>(-CO<sub>2</sub><sup>-</sup>) = 1431*s*; ν(=C-N) = 1360-1200*m-s*; ν(C-N) = 1173*w* and 1144*w*; δ(N-H) = 738*m*.

**3**: ν(N-H) = 3334*m*; ν(-CH<sub>2</sub>-) = 2994*w*; ν(C=O) = 1751*w*; ν(-CO<sub>2</sub><sup>-</sup>) = 1571*vs*; ν<sub>asym</sub>(-CO<sub>2</sub><sup>-</sup>) = 1517*s*; ν<sub>sym</sub>(-CO<sub>2</sub><sup>-</sup>) = 1431*s*; ν(=C-N) = 1360-1200*m-s*; ν(C-N) = 1172*w* and 1144*w*; δ(N-H) = 738*m*.

## 2.5. Single-Crystal X-ray Diffraction

Single-crystals of 2-chloro-4,6-bis(methoxycarbonylmethylamine)-1,3,5-triazine (**L'**), 4,6-bis(carboxymethylamino)-2-oxo-2,3-dihydro-1,3,5-triazin-1-ium chloride (H<sub>2</sub>bodt·HCl) and [La(bodt)(Hbodt)] (**1**) suitable for single-crystal X-ray analysis were harvested and mounted on Hampton

Research CryoLoops using a highly viscous FOMBLIN Y perfluoropolyether vacuum oil (LVAC 140/13) purchased from Sigma-Aldrich with the help of a Stemi 2000 stereomicroscope equipped with Carl Zeiss lenses.<sup>29</sup> Complete diffraction data sets were collected at 150(2) K on a Bruker X8 Kappa APEX II charge-coupled device (CCD) area-detector diffractometer (Mo  $K_{\alpha}$  graphite-monochromated radiation,  $\lambda = 0.7107 \text{ \AA}$ ) controlled by the APEX2 software package,<sup>30</sup> and equipped with an Oxford Cryosystems Series 700 cryostream monitored remotely by the software interface Cryopad.<sup>31</sup> Images were processed using the software package SAINT+,<sup>32</sup> and data were corrected for absorption by the multi-scan semi-empirical method implemented in SADABS.<sup>33</sup> Structures were solved using the direct methods implemented in SHELXS-97,<sup>34</sup> which allowed the immediate location of the majority of the atoms. All remaining non-hydrogen atoms were directly located from difference Fourier maps calculated from successive full-matrix least squares refinement cycles on  $F^2$  using SHELXL-97.<sup>34a, 35</sup> Non-hydrogen atoms of all compounds were successfully refined using anisotropic displacement parameters.

Hydrogen atoms bonded to aromatic carbon were located at their idealized positions using appropriate *HFIX 43* instructions in SHELXL: *43* for the aromatic atoms, *137* for the terminal methyl groups, and *23* for the  $-\text{CH}_2-$  moieties. All hydrogen atoms have been treated as riding on their parent atoms in subsequent refinement cycles of the structural models, with isotropic thermal displacement parameters ( $U_{\text{iso}}$ ) fixed at 1.2 (aromatic and  $-\text{CH}_2-$ ) or 1.5 (methyl groups) times  $U_{\text{eq}}$  of the carbon atom to which they are attached.

Hydrogen atoms associated with nitrogen were markedly visible from difference Fourier maps, and were included in the final structural models with the N–H distances restrained to  $0.95(1) \text{ \AA}$  (in order to ensure a chemically reasonable geometry for these molecules), and by assuming a riding-motion approximation with an isotropic thermal displacement parameter fixed at 1.5 times  $U_{\text{eq}}$  of the nitrogen atom to which they are attached.

The last difference Fourier map synthesis showed: for  $L'$ , the highest peak ( $0.576 \text{ e\AA}^{-3}$ ) and deepest hole ( $-0.382 \text{ e\AA}^{-3}$ ) located at  $1.04 \text{ \AA}$  and  $0.67 \text{ \AA}$  from Cl1; for  $\text{H}_2\text{bodt}\cdot\text{HCl}$ , the highest peak ( $0.469 \text{ e\AA}^{-3}$ ) and deepest hole ( $-0.254 \text{ e\AA}^{-3}$ ) located at  $0.74 \text{ \AA}$  and  $0.82 \text{ \AA}$  from C4 and C7, respectively; for **1**, the highest peak ( $1.110 \text{ e\AA}^{-3}$ ) and deepest hole ( $-1.202 \text{ e\AA}^{-3}$ ) located at  $1.85 \text{ \AA}$  and  $1.18 \text{ \AA}$  from C3 and La1, respectively.

Information concerning crystallographic data collection and structure refinement details is summarized in Table 1. Hydrogen bonding geometric details for the three structures are provided in Tables 2, 3 and 5, while selected bond lengths and angles for the  $\text{La}^{3+}$  (in **1**) coordination environment are collected in Table 4. Structural drawings have been prepared using the software package Crystal Diamond.<sup>36</sup>

→ **Insert Table 1** ←

Crystallographic data (excluding structure factors) for the single-crystal structures reported in this paper have been deposited with the Cambridge Crystallographic Data Centre (CCDC) as supplementary publication Nos. CCDC-988891 (**L'**), -988890 (H<sub>2</sub>bodt·HCl) and -988889 (**1**). Copies of available data can be obtained free of charge on application to CCDC, 12 Union Road, Cambridge CB2 2EZ, UK; FAX: (+44) 1223 336033, or online via [www.ccdc.cam.ac.uk/data\\_request/cif](http://www.ccdc.cam.ac.uk/data_request/cif) or by emailing [data\\_request@ccdc.cam.ac.uk](mailto:data_request@ccdc.cam.ac.uk).

## 2.6. Photoluminescence

The emission and excitation spectra were recorded at 12 and 295 K using a Fluorolog-2<sup>®</sup> Horiba Scientific (Model FL3-2T) spectroscopy, with a modular double grating excitation spectrometer (fitted with a 1200 grooves/mm grating blazed at 330 nm) and a TRIAX 320 single emission monochromator (fitted with a 1200 grooves/mm grating blazed at 500 nm, reciprocal linear density of 2.6 nm mm<sup>-1</sup>), coupled to a R928 Hamamatsu photomultiplier, using the front face acquisition mode. The excitation source was a 450 W Xe arc lamp. Emission spectra were corrected for the detection and optical spectral response of the spectrofluorimeter, and the excitation spectra were corrected for the spectral distribution of the lamp intensity using a photodiode reference detector. Time-resolved measurements have been carried out using a 1934D3 phosphorimeter coupled to the Fluorolog<sup>®</sup>-3, and a Xe-Hg flash lamp (6 μs/pulse half width and 20-30 μs tail) was used as the excitation source. The measurements at 12 K were performed using a helium-closed cycle cryostat with vacuum system measuring ~10<sup>-6</sup> mbar and a Lakeshore 330 auto-tuning temperature controller with a resistance heater.

## 2.7. Time-dependent density functional theory (TD-DFT) calculations

Recent investigations have shown that the B3LYP functional<sup>37</sup> is reliable for describing the geometrical parameters and electronic structure of lanthanide complexes.<sup>28</sup> Thus, we employed a B3LYP/ECP/6-31g\* approach to describe the La<sup>3+</sup> ion (effective core potential by Dolg *et al.*)<sup>38</sup> for the structure and ligand-based properties. The geometry optimizations in the gas-phase and without symmetry constraints for the ground-state singlet (*S*<sub>0</sub>) and lowest-lying singlet excited state (*S*<sub>1</sub>) were performed using DFT and TD-DFT<sup>39</sup> methods, respectively. Harmonic vibrational frequencies were calculated at the same level for all optimized structures, which were shown to have no negative eigenvalues for the Hessian matrices. Using the *S*<sub>0</sub> structure, the vertical electronic excitation energies related to the singlet and triplet states were obtained by TD-DFT calculations at the same level as the geometry optimization. Oscillator strengths were deduced from the dipole transition matrix elements (for singlet states only). The fluorescence electronic transitions were calculated as vertical de-excitations

based on the TD-DFT-optimized geometry of the  $S_1$  state. All the quantum chemistry calculations were performed with Gaussian 09W - Revision A.02 program using its default criteria.<sup>40</sup>

## 3. Results and discussion

### 3.1. Synthesis

#### *Design of 4,6-bis(carboxymethylamino)-2-oxo-2,3-dihydro-1,3,5-triazin-1-ium chloride*

The research groups of Bai and Scheer<sup>25b-d</sup> described the synthesis of novel transition metal coordination polymers with the tripodal *N,N',N''*-1,3,5-triazine-2,4,6-triyltris-glycine ligand. In these reports the authors refer to the preparation of this molecule as based on a patented procedure by Clark in the beginning of the 80s.<sup>41</sup> Because our aim was to solely isolate the disubstituted form (*i.e.*, the bipodal ligand), 4,6-bis(carboxymethylamino)-2-oxo-2,3-dihydro-1,3,5-triazin-1-ium chloride ( $H_2bodt \cdot HCl$ ), we have designed and optimized a new synthetic route whose details are depicted in Scheme 1.

→ **Insert Scheme 1** ←

2-Chloro-4,6-bis(methoxycarbonylmethylamine)-1,3,5-triazine (**L'**) was prepared, in a first step, via the nucleophilic substitution of cyanuric chloride with glycine methyl ester hydrochloride,<sup>42</sup> being isolated in 62% yield. We note that performing the same reaction in dried toluene systematically led to the formation of a mixture of the three possible organic substituted molecules (please note: **L'** was isolated as a minor product in just 16% yield).<sup>43</sup> In this way, time-consuming separations by flash column chromatography were needed. The synthetic route reported in this paper (acetone as the solvent at ambient temperature – see Experimental Section for additional details) was chosen after a careful optimization of a handful of reaction parameters, leading to a straightforward method to obtain **L'** in good reaction yields (62%).

Compound **L'** could be seamlessly converted into  $H_2bodt \cdot HCl$  in quantitative yields by acid hydrolysis using HCl (6 M) at reflux (see Experimental Section). This procedure promotes the total hydrolysis of the ester groups and a complete conversion to the corresponding carboxylic acid form, readily available to coordinate to metallic centres (a pre-requisite for the preparation of coordination polymers). We note that alkaline hydrolysis conditions using a methanolic solution of potassium hydroxide was also attempted during our investigations (data not shown), but it was discarded as a reliable route: using this method the final hydrolyzed compound systematically crystallized with KOH in a non-stoichiometric fashion. The presence of KOH also proved to have a strong influence in the initial pH of the prepared reactive mixtures for the hydrothermal synthesis, ultimately leading to poorly reproducible preparation methods.

Both compounds, including their crystalline structures (see sub-section 3.2), have been characterized in detail by NMR spectroscopy and mass spectrometry (see Figs. S1-S6 in the ESI).

### **Conventional Hydrothermal Synthesis of Isotypical [Ln(bodt)(Hbodt)] Materials**

The preparation of three isotypical materials, formulated as [La(bodt)(Hbodt)] [where  $\text{Ln}^{3+} = \text{La}^{3+}$  (**1**),  $(\text{La}_{0.95}\text{Eu}_{0.05})^{3+}$  (**2**) and  $(\text{La}_{0.95}\text{Tb}_{0.05})^{3+}$  (**3**)], was based on traditional hydrothermal synthesis combining the organic linker  $\text{H}_2\text{bodt}\cdot\text{HCl}$  with the respective lanthanide (III) chloride hydrates (see Experimental Section for details). To derive which conditions maximized the overall crystallinity of the final products, several reaction conditions were systematically optimized: the reaction temperature was varied between 120 and 180 °C; water (hydrothermal) and dimethylformamide (solvothermal) were employed as solvents; the inclusion of triethylamine as a reactant (*ca.* 1.5 molar ratio with respect to the organic ligand) was also investigated. We found that phase purity and crystallinity were usually promoted at lower temperatures and when water was employed as the solvent. Noteworthy, these results are in good agreement with the conclusions derived by Bai & Scheer<sup>25b-d</sup> when using *N,N',N''*-1,3,5-triazine-2,4,6-triyltrisglycine. We found that for higher temperatures either no solid product could be isolated from the reaction vessels or the partial destruction of the organic ligand occurred with the product exhibiting poor crystallinity and a brownish color. The use of dimethylformamide systematically led to poor crystalline materials.

The phase purity and homogeneity of the bulk compounds **1-3** were investigated by using standard solid-state techniques: elemental analysis, electron microscopy (Figs. S7 and S8 in the ESI), thermogravimetry (Fig. S14 in the ESI) and FT-IR (Fig. S15 in the ESI).

Compound **1** was isolated as suitable single-crystals for X-ray diffraction studies (see sub-section 3.2). Phase identification of the mixed-lanthanide materials **2** and **3** was performed by powder X-ray diffraction (PXRD) that unequivocally proved that both compounds share the same crystalline phase with **1** (Fig. 1). Morphologically, compounds **1-3** have quite similar crystal habit (Fig. 1): all materials are composed of aggregates of well-defined plate-like particles.

→ Insert Figure 1 ←

### **3.2. Crystal Structure Description**

The crystal structures of the intermediate 2-chloro-4,6-bis(methoxycarbonylmethylamine)-1,3,5-triazine (*L'*), 4,6-bis(carboxymethylamino)-2-oxo-2,3-dihydro-1,3,5-triazin-1-ium chloride ( $\text{H}_2\text{bodt}\cdot\text{HCl}$ ) and [La(bodt)(Hbodt)] (**1**) were unveiled by single-crystal X-ray diffraction (Table 1). In the next paragraphs, and also following our interest in the structural features of organic crystals,<sup>44</sup> some crystallographic features belonging to each compound will be highlighted.

→ Insert Table 1 ←

## ***2-Chloro-4,6-bis(methoxycarbonylmethylamine)-1,3,5-triazine (L')***

The crystal structure of the intermediate *L'* molecule (see Scheme 1) was determined in the centrosymmetric monoclinic  $P2_1/n$  space group. The asymmetric unit is composed of a whole molecular unit as depicted in Fig. 2a. Despite the bulk nature of the two pendant substituent groups of the aromatic ring, these are pointing towards the same side of the aromatic ring, with this conformation promoting an effective crystal packing. In addition, when combined with the mutual rotation of the two terminal ester groups, this conformation further allows the existence of two weak C–H $\cdots$ O hydrogen bonding interactions [not shown;  $d_{D\cdots A}$ : ca. 3.32–3.35 Å;  $\angle(\text{DHA})$  angles: ca. 117–130°] between the two terminal groups, further helping in the stabilization of this conformation in the solid state.

→ **Insert Figure 2** ←

Neighboring molecules of *L'* interact via strong ( $d_{D\cdots A}$  of ca. 2.63 Å) and highly directional [ $\angle(\text{DHA})$  angles close to linearity – see Table 2] N–H $\cdots$ N hydrogen bonding interactions involving the N–H moieties of the pendant groups (donors) and the closest nitrogen atom from the adjacent aromatic ring (acceptors). This leads to a typical  $\mathbf{R}_2^2(8)$  graph set motif<sup>45</sup> which repeats itself in a recursive fashion being, in this way, at the genesis of a one-dimensional supramolecular zigzag tape as represented in Fig. 2b. Because each pair of adjacent molecular units of *L'* are related by inversion, the pendant groups point in an alternate fashion with respect to the plane of the supramolecular tape. This leads to two important features in the crystal structure. First, it promotes the presence of weak C–H $\cdots$ Cl contacts [not shown;  $d_{D\cdots A}$ : ca. 3.85–3.90 Å;  $\angle(\text{DHA})$  angles: ca. 138–143°] which strengthen the aforementioned  $\mathbf{R}_2^2(8)$  graph set motifs. Second, it seems to help the effectiveness of the crystal packing because adjacent tapes can easily fit onto each other based on purely geometrical reasons (Fig. S9a in the ESI). It is also worth to emphasize that the aromatic rings belonging to each pair of supramolecular tapes are further engaged in  $\pi$ - $\pi$  contacts, with the distance between the average planes being of about 3.4 Å (Fig. S9b in the ESI).

→ **Insert Table 2** ←

The close packing of the supramolecular tapes occurs in a typical ABAB $\cdots$  fashion along the crystallographic [010] direction (Fig. S10 in the ESI), with the interactions between adjacent tapes being mainly of weak nature: van der Waals and several C–H $\cdots$ O contacts involving solely the pendant groups of the individual molecular units.

**4,6-bis(carboxymethylamino)-2-oxo-2,3-dihydro-1,3,5-triazin-1-ium chloride (H<sub>2</sub>bodt·HCl)**

The hydrolysis in acidic medium of the intermediate *L'* molecule (Scheme 1) leads to a new protonated molecular unit, C<sub>7</sub>H<sub>10</sub>N<sub>5</sub>O<sub>5</sub><sup>+</sup> (Fig. 3a). The crystal charge is balanced by the presence of a crystallographically independent chloride anion which is liberated from the molecular unit of *L'* with the concomitant oxidation of the ring to a C=O bond. The compound is, thus, a salt with empirical formula C<sub>7</sub>H<sub>10</sub>N<sub>5</sub>O<sub>5</sub>Cl: H<sub>2</sub>bodt·HCl. It is of considerable importance to emphasize that this oxidation of the ring is accompanied by the destruction of its aromatic nature with the appearance of one N–H bond. We further note that the second N–H bond arises from the presence of the required proton to balance the crystal charge. Just like in *L'*, the two pendant substituent groups are pointing towards the same side of the ring, but no mutual interactions were observed. Instead, the average planes containing the two terminal carboxylic acid groups are almost parallel with the mutual dihedral angle being of about 12°.

→ **Insert Figure 3** ←

When compared to *L'*, the supramolecular contacts in H<sub>2</sub>bodt·HCl are strikingly different. The charged nature of the organic unit leads to the disruption of the **R**<sub>2</sub><sup>2</sup>(8) graph set motifs<sup>45</sup> connecting adjacent molecules in *L'*, with the chloride anion being now intercalated in-between neighboring units (Fig. 3b). The two bridging **R**<sub>2</sub><sup>2</sup>(6) motifs are formed by strong (*d*<sub>D...A</sub> of *ca.* 3.07-3.34 Å) and directional [ $\angle$ (DHA) angles above 145° – see Table 3] N–H...Cl hydrogen bonding interactions. These connections form, in a first stage, zigzag tapes which are more distorted than those observed in the previous structure due to the intercalation of the anion. Furthermore, this intercalation brings to a close proximity the C=O moiety of one molecule and one –CH<sub>2</sub>– group of an adjacent one (Fig. 3b), leading to the presence of weak C–H...O contacts [not shown; *d*<sub>D...A</sub> of *ca.* 3.18 Å;  $\angle$ (DHA) angle of *ca.* 155°] which strengthens the interactions between adjacent cationic molecular units.

→ **Insert Table 3** ←

The two terminal carboxylic acid groups are engaged in typical **R**<sub>2</sub><sup>2</sup>(8) graph set motifs with related groups from a neighbor supramolecular tape. These O–H...O hydrogen bonding interactions are considerably strong (*d*<sub>D...A</sub> of *ca.* 2.63 Å – see Table 3) and highly directional [ $\angle$ (DHA) angles of *ca.* 177°], forming staircase-like layers as depicted in Fig. 3c. In addition, offset  $\pi$ - $\pi$  stacking interactions are present between adjacent supramolecular tapes with an average inter-plane distance of about 3.71 Å (Fig. S11 in the ESI). These supramolecular interactions play a decisive role in the crystal packing of the

supramolecular salt  $\text{H}_2\text{bodt}\cdot\text{HCl}$  with an alternation along the [100] crystallographic direction of  $\mathbf{R}_2^2(8)$  graph set motifs and  $\text{N}-\text{H}\cdots\text{Cl}$  hydrogen bonding interactions (see Fig. S12 in the ESI).

### **Coordination Polymer [La(bodt)(Hbodt)] (1)**

The reaction between  $\text{H}_2\text{bodt}\cdot\text{HCl}$  with lanthanum chloride under typical hydrothermal conditions (see Experimental Section for further details on the synthesis), led to the isolation of a highly crystalline material which was formulated as  $[\text{La}(\text{bodt})(\text{Hbodt})]$  (**1**) (where  $\text{bodt}^{2-}$  stands for fully deprotonated ligand resultant from the neutral  $\text{H}_2\text{bodt}$  molecule) on the basis of single-crystal X-ray diffraction studies.

The asymmetric unit of **1** comprises a  $\text{La}^{3+}$  metallic centre located at a special crystallographic position (on a two-fold axis) and a whole organic ligand in which the N4 atom is partially protonated (rate of occupancy of 50%) as depicted in Fig. 4a. The spatial distribution of the coordinating pendant substituents of the ligand, in combination with their structural conformational flexibility, allows the connection of this organic primary building block via two *syn,syn*-chelates (Fig. 4a), with the pendant groups resembling structural “claws”. The “bite” angles of these coordinating groups were found in the  $48.32(10)$ - $49.78(11)^\circ$  range (Table 4), being typical of this structural arrangement as revealed by a systematic search in the Cambridge Structural Database.<sup>46</sup>

→ **Insert Figure 4** ←

→ **Insert Table 4** ←

The coordination sphere of the  $\text{La}^{3+}$  centre is composed of four symmetry-related organic ligands as represented in Fig. 4b. Two molecules exhibit the coordination modes described in the previous paragraph, and the other two result from the *syn*-bridging fashion of O4 that is the responsible for the formation of the polymeric structure present in **1** (see below). The metallic centre is, thus, coordinated to a total of 10 oxygen atoms,  $\{\text{LaO}_{10}\}$ . The La–O bond lengths range from 2.528(3) to 2.713(3) Å (Table 4), with the latter distance being related to the *syn*-bridge of O4 that connects adjacent  $\text{La}^{3+}$  metallic centres. Noteworthy, by considering the centres of gravity of the *syn,syn*-chelated carboxylate groups as the vertices, the coordination polyhedron can be envisaged as a highly distorted octahedron (Fig. 4c) with the *cis* and *trans* internal angles found in the *ca.*  $76.2$ - $110.0^\circ$  and  $154.1$ - $179.6^\circ$  ranges, respectively.

The most striking structural feature of compound **1** resides in the presence of a one-dimensional  $\infty^1[\text{La}(\text{bodt})(\text{Hbodt})]$  coordination polymer running parallel to the [001] direction of the unit cell (Fig. 5). This polymer is formed by the carboxylate “claw” C7 that has the oxygen atom O4 establishing a physical bridge with a neighbouring metallic centre (related to the first by inversion), ultimately imposing  $\text{La}\cdots\text{La}$  intermetallic distance of 4.4279(7) Å (Fig. 5a) along the growing direction of the polymer.

→ **Insert Figure 5** ←

Adjacent  $\infty^1[\text{La}(\text{bodt})(\text{Hbodt})]$  coordination polymers are engaged in strong [ $d_{\text{D}\cdots\text{A}}$ : 2.755(8)-2.859(5) Å] and close-to-linear [ $\langle(\text{DHA})$  angles: 174-176° - see Table 5] N–H $\cdots$ (N,O) hydrogen bonding interactions involving spatially-close organic rings (Fig. 6a). This leads to the formation of cooperative  $\mathbf{R}_2^2(8)$  graph set motifs<sup>45</sup> which recursively repeat along the polymeric chain (Fig. 6b). Consequently, each  $\infty^1[\text{La}(\text{bodt})(\text{Hbodt})]$  polymer is physically connected to another adjacent symmetry-related four entities (Fig. 6c), with this feature being at the genesis of a “hybrid” supramolecular network composed of coordinative bonds alternating with hydrogen bonding interactions. Noteworthy, the crystal structure of **1** is formed by a two-fold interpenetration of such identical entities, with physical connections between adjacent networks being essentially ensured by bifurcated, slightly weaker, N–H $\cdots$ O hydrogen bonding interactions (Fig. S13a in the ESI): on the one hand, the  $d_{\text{D}\cdots\text{A}}$  distances are slightly longer, 2.821(5)-2.970(6) Å, and, on the other, they deviate from linearity with the highest  $\langle(\text{DHA})$  angle being of only 150° (Table 5). Besides these interactions, the close proximity of the organic ligands leads to the presence of weak interactions with the average planes (containing the organic rings) being as close as *ca.* 3.2 Å (Fig. S13b in the ESI).

→ **Insert Figure 6** ←→ **Insert Table 5** ←

The self-organization of the  $\infty^1[\text{La}(\text{bodt})(\text{Hbodt})]$  coordination polymers mediated via the supramolecular contacts described in the previous paragraphs leads to the formation of a compact structure as represented in Fig. 7. It is interesting to note the presence of clear frontiers between the organic and the inorganic components of the supramolecular structure: molecular “wires” of lanthanum oxide are embedded into an organic matrix composed by the rings of the organic building block.

→ **Insert Figure 7** ←

### 3.3. Thermogravimetry and Vibrational Spectroscopy

The thermal stability of the  $[\text{Ln}(\text{bodt})(\text{Hbodt})]$  materials [where  $\text{Ln}^{3+} = \text{La}^{3+}$  (**1**),  $(\text{La}_{0.95}\text{Eu}_{0.05})^{3+}$  (**2**) and  $(\text{La}_{0.95}\text{Tb}_{0.05})^{3+}$  (**3**), was investigated between ambient temperature and 650 °C. The thermograms (see Fig. S14 in the ESI) show that the three materials have a very similar thermal behaviour. The crystalline structures remain thermally stable up to approximately 300 °C, after which temperature and up to *ca.* 650 °C the overall thermal decomposition occurs in two main consecutive steps corresponding to total weight losses of *ca.* 67.8, 70.9 and 70.2% for materials **1**, **2** and **3**, respectively.

FT-IR spectroscopy gives further evidence that the bulk materials **1-3** are indeed isotypical, with the spectra (Fig. S15 in the ESI) exhibiting several diagnostic vibrational modes characteristic of the various functional groups composing the materials. Because the FT-IR spectra of the three compounds are quite similar, in the following paragraphs we shall only discuss in detail the spectral features of compound **1**, being the derived considerations also valid for compounds **2** and **3**.

The typical vibration bands, of medium intensity, belonging to the  $\nu(-\text{NH})$  stretching modes appear at *ca.*  $3334\text{ cm}^{-1}$ . A weak and sharp band corresponding to the  $\nu(-\text{CH}_2-)$  vibrational modes are centered at *ca.*  $2992\text{ cm}^{-1}$ . The  $\nu(\text{C}=\text{O})$  stretching vibrational modes arising from both the carbonyl presented in the ring and those in the carboxylate groups peak at *ca.*  $1752\text{ cm}^{-1}$ .<sup>25d, 47</sup>

The carboxylate ( $-\text{CO}_2^-$ ) groups may coordinate to the metallic centers in different ways: monodentate, chelating bidentate or bridging bidentate modes. The wavenumber separation ( $\Delta\nu_{\text{asym-sym}}$ ) between the asymmetric and symmetric stretching vibrational modes of carboxylate group varies according to the coordination mode. While the wavenumber separation in bridging bidentate fashion varies usually between  $120$  and  $160\text{ cm}^{-1}$ , in chelating bidentate mode the value is lower.<sup>48</sup> The FT-IR spectrum of **1** shows a pair of bands located at around  $1517$  and  $1431\text{ cm}^{-1}$ , which are attributed to asymmetric and symmetric stretching vibrations modes of the  $-\text{CO}_2^-$  group, respectively. This feature is indicative that some carboxylate groups are coordinated to the metal center through chelating bidentate mode ( $\Delta\nu_{\text{asym-sym}} \approx 85\text{ cm}^{-1}$ ), which is in good agreement with the single-crystal X-ray diffraction studies.

Additionally, the set of vibration bands of medium-to-strong intensity attributed to the  $\nu(\text{C}=\text{N})$  stretching modes appear in the  $1360$ - $1200\text{ cm}^{-1}$  spectral range, followed by two bands at *ca.*  $1173$  and  $1144\text{ cm}^{-1}$  attributed to  $\nu(\text{C}-\text{N})$ . The  $\delta(\text{N}-\text{H})$  vibrational mode appears at  $738\text{ cm}^{-1}$ .<sup>47</sup>

### 3.4. Photoluminescence spectroscopy and TD-DFT calculations

The photoluminescent properties of the optically active  $[(\text{La}_{0.95}\text{Eu}_{0.05})(\text{bodt})(\text{Hbodt})]$  (**2**) and  $[(\text{La}_{0.95}\text{Tb}_{0.05})(\text{bodt})(\text{Hbodt})]$  (**3**) materials were investigated at ambient and low temperatures. Some observed experimental data is further supported by time-dependent density functional theory studies (TD-DFT). The excitation spectrum of **2** recorded at ambient temperature (Fig. 8) displays a series of sharp lines assigned to the  ${}^7\text{F}_{0-1} \rightarrow {}^5\text{D}_{4-0}$ ,  ${}^5\text{L}_6$ ,  ${}^5\text{G}_{2-6}$ ,  ${}^5\text{H}_{3-7}$  and  ${}^5\text{F}_{1-5}$   $\text{Eu}^{3+}$  intra- $4f^6$  transitions. On the high energy region the spectrum exhibits an additional broad band, peaking at  $275\text{ nm}$ , tentatively attributed to the  $\pi-\pi^*$  transitions associated with the organic linkers. At low temperature ( $12\text{ K}$ ) an additional intense broad band peaking at  $255\text{ nm}$  appears, attributable to the organic linker, which completely dominates the  $12\text{ K}$  excitation spectra. The increasing intensity of the  $255\text{ nm}$  broad band with decreasing temperature demonstrates a non-effective energy transfer from the ligand to the  $\text{Eu}^{3+}$  ions (*antenna effect*) at ambient temperature. The attribution of these UV bands has been confirmed by investigating the excitation

spectrum of the pure  $\text{La}^{3+}$ -based material,  $[\text{La}(\text{bodt})(\text{Hbodt})]$  (**1**), recorded at 12 K while monitoring the phosphorescence emission at 420 nm (see Fig. S16).

Fig. 9 shows the emission spectra of **2** excited at 394 nm. The sharp lines are assigned to transitions between the first excited non-degenerate  $^5\text{D}_0$  state and the  $^7\text{F}_{0-4}$  levels of the fundamental  $\text{Eu}^{3+}$  septet. The local-field splitting of the  $^7\text{F}_{1,2}$  levels in three and five Stark components, respectively, the presence of a single line for the  $^5\text{D}_0 \rightarrow ^7\text{F}_0$  transition and the predominance of the  $^5\text{D}_0 \rightarrow ^7\text{F}_2$  transition supports the presence of a single low-symmetry  $\text{Eu}^{3+}$  environment, as indicated by the crystal structure investigations (see previous sections for details). Independently of the line detected and for a direct excitation at 394 nm ( $^5\text{L}_6$  excited level), the  $^5\text{D}_0$  decay curves of  $\text{Eu}^{3+}$  at ambient temperature (295 K) and 12 K give the same single lifetime of  $1.38 \pm 0.01$  ms (Fig. S17), further corroborating the detection of a single  $\text{Eu}^{3+}$  ion in the crystal structure and indicating an absence of the suppression of the  $\text{Eu}^{3+}$  emission *via* the vibrations of the coordinated ligands.

To better understand the non-effective ambient temperature ligand-to- $\text{Eu}^{3+}$  energy transfer in compound **2**, we have investigated in more detail the luminescence of the pure  $\text{La}^{3+}$ -based compound. As depicted in Fig. S16 (see the ESI), the  $\text{La}^{3+}$ -based compound at 12 K presents a broad emission band in the range of 270 to 590 nm, peaking at *ca.* 390 nm, when excited at 255 nm. As demonstrated by the stationary state and time-resolve emission modes, this emission band is composed by a fast component in the high energy range most probably due to the singlet fluorescence emission of the ligand, and by a slower part on the lower energy range attributable to the triplet phosphorescence emission. Moreover, the singlet fluorescence emission spectra exhibit also a small and very narrow peak near the emission maximum (at *ca.* 367 nm). Therefore, the presence of the different chemical components within the organic ligand, namely a carboxymethylamino group and a triazine-derivative ring, that can also be associated with different electronic excited states, seems a plausible explanation to justify the presence of different fluorescence emissions.

Due to the energy resonance between the triplet level and the first  $\text{Eu}^{3+}$  emitting level ( $^5\text{D}_0$  at *ca.* 578 nm), it is possible to occur a back energy transfer between the  $\text{Eu}^{3+}$  and the ligand followed by non-radiative relaxation. This back energy transfer, not detectable in the ambient temperature  $\text{Eu}^{3+}$  emission spectrum, is well observable in the ambient temperature emission spectrum of the  $\text{Tb}^{3+}$ -based material **3** (Fig. S18 in the ESI), which shows a faint broad emission peaking at *ca.* 420 nm. Note that the corresponding excitation spectrum lines can be exclusively attributed to intra-configurational  $4f^8 \rightarrow 4f^8$  and inter-configurational  $4f^8 \rightarrow 4f^7 5d^1$  transitions of  $\text{Tb}^{3+}$  ions.<sup>49</sup>

When compound **1** was excited at 306 nm very narrow lines were observed in both emission spectra at 12 K and at ambient temperature (Fig. 10). At ambient temperature a set of well-defined sharp emission lines in the 370 to 400 nm region was observed (Fig. 10), having a short lifetime of *ca.* 8  $\mu\text{s}$  estimated at their maximum (see details in Fig. S19 in the ESI). The corresponding excitation spectrum is

dominated by an intense sharp line peaking at *ca.* 306 nm and a faint sharp one at *ca.* 313 nm (Fig. 10). At 12 K only two sharp emission lines are visible, one intense at *ca.* 367.5 nm (the small one already observed at 12 K but when excited at 255 nm; Fig. S16), and another relatively faint at *ca.* 373.3 nm, which appears superimposed to the conventional broad emission band of the ligand. The disappearance of the ambient temperature structured emission sharp emission lines is most probably due to the Boltzmann depopulation of the upper fundamental states with the decrease in temperature. A tentative simplified energy scheme of both the ambient temperature and 12 K emission processes is given in Fig. S20 (in the ESI).

The line widths in the emission spectra of organic compounds are typically of a few hundred of wavenumbers, even at ultra-low temperatures. A strong decrease in the line widths can even be observed if the molecules are embedded in the lattice of a host crystal with a well-defined fit of the guest molecule in the crystalline matrix.<sup>50</sup> In this context, the rigid crystal structure of compound **1** described in the previous sections can ultimately be considered a Shpol'skii matrix, with the organic ligands being envisaged as guest molecules trapped in the polymeric host matrix.<sup>51</sup> Thus, the observed sharp emission lines can be associated to Shpol'skii-type fluorescence emission spectra,<sup>52</sup> which imply site-specific selection within **1**.

To better understand the nature of the observed anomalous emission and excitation fluorescence spectra (in particular, the very narrow excitation bandwidth at ambient temperature – see Fig. 10), similar photoluminescence experiments were performed on the precursor supramolecular salt 4,6-bis(carboxymethylamino)-2-oxo-2,3-dihydro-1,3,5-triazin-1-ium chloride ( $H_2bodt \cdot HCl$ ). Experimental data (not shown) did not provide similar emission or excitation spectra. The enhancement of the emission efficiency can be attributed to the coordination of the ligand to the metallic centers, effectively increasing the rigidity of the organic PBUs and reducing the loss of energy via radiation-less decay of the intra-ligand emission excited state.

From the crystallographic studies performed, the crystal packing of compound **1** is strongly based on cooperative N–H $\cdots$ (N,O) hydrogen bonds possessing very close proton donor and acceptor groups, in particular the connections between adjacent  $\infty^1[La(bodt)(Hbodt)]$  coordination polymers (Fig. 6). These connections are completely absent from the structure of  $H_2bodt \cdot HCl$  by the presence of the charge-balancing chloride anion. Realizing that the observed emissive excited states (at both 12 K and ambient temperature) lies in the hydrogen-bonded structure, a proposal of excited-state intermolecular proton transfer (ESPT) process involving the N-H and C=O groups in **1** at ambient temperature is suggested, with the emissive excited states being ascribed to a excited tautomeric structure. The observed narrow excitation bandwidth is similar to reported values for an ESPT process.<sup>53</sup> In addition, this process was also verified in other coordination polymers.<sup>54</sup> The short lifetime of *ca.* 8  $\mu s$  (Fig. S19) is also within the range observed at ESPT processes.<sup>55</sup> We note that this excited tautomeric structure cannot be readily

achieved in a frozen matrix because a molecular rearrangement is required, hence the absence of a similar narrow excitation bandwidth at 12 K.

To gain insight into the photophysical behaviour of compound **1**, methods based on density functional theory (DFT) together with its time-dependent formalism (TD-DFT) were applied. Because the calculation of the excited state requires significantly much more computational demand than that of the ground state, theoretical calculations were performed on a simplified model (Fig. 11) based on the hydrogen-bonded structure obtained from the crystallographic studies of compound **1**. It should be emphasized that, due to the good agreement between experimental and theoretical results (discussed hereinafter), this simplified model efficiently represents the real system with respect to the electronic properties.

To further understand the fundamental aspects concerning the emission features, geometry optimizations for the ground-state singlet ( $S_0$ ) and lowest-lying singlet excited state ( $S_1$ ) of the simplified model were performed (Fig. 11). Comparing the  $S_0$  and  $S_1$  geometries permits to infer that when the hydrogen-bonded structure is excited to the  $S_1$  state the intermolecular N–H $\cdots$ O hydrogen bonds are liable to undergo excited-state proton transfer. As the bond lengths of the C=O moieties are slightly increased (from 1.217/1.239 Å in the  $S_0$  to 1.220/1.242 Å in  $S_1$  states), non-bonding electrons of –NH– nitrogen can be promoted to the  $\pi^*$  orbitals of the C=O oxygen. The –NH– proton migrates to the C=O oxygen in the excited state from  $S_1$  to  $S_1^*$  leading to an excited tautomeric state. Then de-excitation takes place, followed by the emission of fluorescence spectra from  $S_1$  to  $S_0$  (observed at 12 K) as well as  $S_1^*$  to  $S_0$  (observed at ambient temperature).

In order to provide a framework for the excited state TD-DFT results, partial molecular orbital compositions relevant to their interpretation are listed in Tables S1 and S2 (in the ESI). The corresponding vertical electronic excitation and de-excitation energies, oscillator strengths and the molecular orbitals mainly involved in selected electronic transitions are listed in Tables S3 and S4 (in the ESI). The vertical excitation energy of the lowest triplet state ( $T_1$ ), calculated to be at 330 nm as a result of electronic excitations involving a HOMO (H) to LUMO (L) transition, compares well with the 328 nm experimental value of the 0-0 onset energy of the triplet phosphorescence emission at 12 K (Fig. S16 in the ESI).

The nature of the emissive excited states in the fluorescence process at 12 K was investigated (Tables S2 and S4 in the ESI) and the identification of the components, carboxymethylamino group or triazine-derivative ring, that give rise to the different emission spectra was theoretically rationalized. Two fluorescence emissions from the same electronic excited state  $S_1$  are expected (see Table S4 in the ESI), a stronger one calculated to occur at 454 nm and the other at 332 nm. From the gathered information summarized in Tables S2 and S4, the emission at 454 nm involves the H-2  $\rightarrow$  L and H-1  $\rightarrow$  L transitions that are assigned to excitations predominantly involving the triazine-derivative ring with, however, some

contributions from the carboxymethylamino group. This emission can be associated with the maximum of the singlet fluorescence emission spectra at 12 K (Fig. S16) and shows quite precise correspondence with the values found for N-heterocyclic triazine-derivatives.<sup>56</sup> The calculated emission at 332 nm also involves transitions that are assigned to excitations predominantly involving the triazine-derivative ring. The contributions from the carboxymethylamino group are however higher than those observed at 454 nm. This emission can be therefore associated with the very narrow peak appearing near the emission maximum when compound **1** is excited at 255 nm (Fig. S16,) corresponding to that intense at *ca.* 367.5 nm when the sample is excited at 306 nm (Fig. 10, 12 K). To intuitively understand the different fluorescence behavior at 12 K depending on the excitation wavelength, the principal singlet-singlet electronic excitation energies (Table S3) were analyzed. Together with the information given in Table S1, it seems that the material emits differently upon excitation at 255 and 306 nm because the associated electronic transitions are predominantly assigned to excitations of triazine-derivative ring and carboxymethylamino group, respectively. Therefore, when the sample is irradiated at 306 nm we are mainly site-specific exciting the groups involved in the hydrogen-bonding interactions and when the temperature is increased (Fig. 10, ambient temperature), the occurrence of an ESPT process becomes possible.

## 4. Concluding Remarks

In this manuscript it was shown that bipodal glycine derivatives could be prepared and used as organic primary building units for the preparation of coordination polymers with lanthanide cations. The supramolecular salt 4,6-bis(carboxymethylamino)-2-oxo-2,3-dihydro-1,3,5-triazin-1-ium chloride ( $\text{H}_2\text{bodt}\cdot\text{HCl}$ ), a precursor of a novel bipodal linker, was prepared in quantitative yields using a simple two-step reaction, for which the precursors and final product were fully characterized in both the solid (X-ray crystallography) and liquid states (NMR spectroscopy and mass spectrometry).

A novel family of isotypical 1D coordination polymers, formulated as  $[\text{Ln}(\text{bodt})(\text{Hbodt})]$  [where  $\text{Ln}^{3+} = \text{La}^{3+}$  (**1**),  $(\text{La}_{0.95}\text{Eu}_{0.05})^{3+}$  (**2**) and  $(\text{La}_{0.95}\text{Tb}_{0.05})^{3+}$  (**3**)] and isolated as large single-crystals, was prepared using conventional static hydrothermal synthesis (120 °C, 48 h). The structural features of the materials have been fully unveiled in the solid state by X-ray diffraction (single-crystal and powder), electron microscopy (SEM and EDS), FT-IR spectroscopy, elemental and thermogravimetric analysis. Crystallographic studies show that compound **1** is based on a one-dimensional  $\infty^1[\text{La}(\text{bodt})(\text{Hbodt})]$  coordination polymer stable up to *ca.* 300 °C, and that the existence of cooperative N–H $\cdots$ (N,O) hydrogen bonding interactions between spatially-close coordination polymers are the main responsible for the formation of a 3D supramolecular structure.

The photoluminescent properties of the mixed-lanthanide compounds **2** and **3** having stoichiometric amounts of the optically-active  $\text{Eu}^{3+}$  and  $\text{Tb}^{3+}$ , respectively, was investigated and compared with the pure  $\text{La}^{3+}$ -based material. These investigations constitute clear evidence for the presence of excited-state intermolecular proton transfer (ESPT) process in **1** at ambient temperature. To further investigate this occurrence we have also performed a theoretical investigation based on time-dependent density functional theory in both the ground and singlet excited states. Derived data fully justify the phosphorescence and fluorescence properties, respectively, of the ligand.

## Acknowledgements

We would like to thank *Fundação para a Ciência e a Tecnologia* (FCT, Portugal), the European Union, QREN, FEDER, COMPETE, *Laboratório Associado Centro de Investigação em Materiais Cerâmicos e Compósitos* - CICECO (Pest C-CTM/LA0011/2013), and the research unit QOPNA (PEst-C/QUI/UI0062/2013) for their general funding scheme. We further wish to thank FCT for the R&D project EXPL/CTM-NAN/0013/2013 (FCOMP-01-0124-FEDER-041282), for granting the funding to build the Iris multi-processor cluster, for the doctoral and post-doctoral research grants Nos. SFRH/BPD/94381/2013 (to SMFV), SFRH/BD/46601/2008 (to PS) and SFRH/BPD/32103/2006 (to MN).

## References

- (a) M. Li, D. Li, M. O'Keeffe and O. M. Yaghi, *Chem. Rev.*, 2014, **114**, 1343-1370; (b) T. R. Cook, Y. R. Zheng and P. J. Stang, *Chem. Rev.*, 2013, **113**, 734-777; (c) G. Férey, *Chem. Soc. Rev.*, 2008, **37**, 191-214; (d) O. M. Yaghi, M. O'Keeffe, N. W. Ockwig, H. K. Chae, M. Eddaoudi and J. Kim, *Nature*, 2003, **423**, 705-714.
- (a) K. Gedrich, M. Heitbaum, A. Notzon, I. Senkowska, R. Frohlich, J. Getzschmann, U. Mueller, F. Glorius and S. Kaskel, *Chem.-Eur. J.*, 2011, **17**, 2099-2106; (b) F. J. Song, C. Wang, J. M. Falkowski, L. Q. Ma and W. B. Lin, *J. Am. Chem. Soc.*, 2010, **132**, 15390-15398; (c) S. Hasegawa, S. Horike, R. Matsuda, S. Furukawa, K. Mochizuki, Y. Kinoshita and S. Kitagawa, *J. Am. Chem. Soc.*, 2007, **129**, 2607-2614; (d) M. J. Katz, J. E. Mondloch, R. K. Totten, J. K. Park, S. T. Nguyen, O. K. Farha and J. T. Hupp, *Angew. Chem., Int. Ed.*, 2014, **53**, 497-501.
- (a) Y. Yan, M. Suyetin, E. Bichoutskaia, A. J. Blake, D. R. Allan, S. A. Barnett and M. Schröder, *Chem. Sci.*, 2013, **4**, 1731-1736; (b) C. E. Wilmer, O. K. Farha, T. Yildirim, I. Eryazici, V. Krungleviciute, A. A. Sarjeant, R. Q. Snurr and J. T. Hupp, *Energy Environ. Sci.*, 2013, **6**, 1158-1163; (c) Z. Y. Guo, H. Wu, G. Srinivas, Y. M. Zhou, S. C. Xiang, Z. X. Chen, Y. T. Yang, W. Zhou, M. O'Keeffe and B. L. Chen, *Angew. Chem., Int. Ed.*, 2011, **50**, 3178-3181; (d) Y. Yan, I. Telepeni, S. H. Yang, X. Lin, W. Kockelmann, A. Dailly, A. J. Blake, W. Lewis, G. S. Walker, D. R. Allan, S. A. Barnett, N. R. Champness and M. Schröder, *J. Am. Chem. Soc.*, 2010, **132**, 4092-4094; (e) S. Q. Ma, D. F. Sun, J. M. Simmons, C. D. Collier, D. Q. Yuan and H. C. Zhou, *J. Am. Chem. Soc.*, 2008, **130**, 1012-1016; (f) K. Lee, W. C. Isley, A. L. Dzubak, P. Verma, S. J. Stoneburner, L. C. Lin, J. D. Howe, E. D. Bloch, D. A. Reed, M. R. Hudson, C. M. Brown, J. R. Long, J. B. Neaton, B. Smit, C. J. Cramer, D. G. Truhlar and L. Gagliardi, *J. Am. Chem. Soc.*, 2014, **136**, 698-704.
- (a) V. Colombo, C. Montoro, A. Maspero, G. Palmisano, N. Masciocchi, S. Galli, E. Barea and J. A. R. Navarro, *J. Am. Chem. Soc.*, 2012, **134**, 12830-12843; (b) A. C. Kizzie, A. G. Wong-Foy and A. J. Matzger, *Langmuir*, 2011, **27**, 6368-6373; (c) O. K. Farha, A. O. Yazaydin, I. Eryazici, C. D. Malliakas, B. G. Hauser, M. G. Kanatzidis, S. T. Nguyen, R. Q. Snurr and J. T. Hupp, *Nat. Chem.*, 2010, **2**, 944-948; (d) D. Britt, H. Furukawa, B. Wang, T. G. Glover and O. M. Yaghi, *Proc. Natl. Acad. Sci.*, 2009, **106**, 20637-20640; (e) D. H. Hong and M. P. Suh, *Chem.-Eur. J.*, 2014, **20**, 426-434.
- (a) Y. C. Chuang, W. L. Ho, C. F. Sheu, G. H. Lee and Y. Wang, *Chem. Commun.*, 2012, **48**, 10769-10771; (b) D. Maspoch, D. Ruiz-Molina, K. Wurst, N. Domingo, M. Cavallini, F. Biscarini, J. Tejada, C. Rovira and J. Veciana, *Nat. Mater.*, 2003, **2**, 190-195.

6. (a) M. Plabst, L. B. McCusker and T. Bein, *J. Am. Chem. Soc.*, 2009, **131**, 18112-18118; (b) T. K. Maji, R. Matsuda and S. Kitagawa, *Nat. Mater.*, 2007, **6**, 142-148; (c) Y. Tasaki-Handa, Y. Abe, K. Ooi, M. Tanaka and A. Wakisaka, *Dalton Trans.*, 2014, **43**, 1791-1796.
7. (a) P. Y. Wu, J. Wang, Y. M. Li, C. He, Z. Xie and C. Y. Duan, *Adv. Funct. Mater.*, 2011, **21**, 2788-2794; (b) Y. Takashima, V. M. Martinez, S. Furukawa, M. Kondo, S. Shimomura, H. Uehara, M. Nakahama, K. Sugimoto and S. Kitagawa, *Nature Communications*, 2011, **2**.
8. (a) J. Rocha, L. D. Carlos, F. A. A. Paz and D. Ananias, *Chem. Soc. Rev.*, 2011, **40**, 926-940; (b) M. D. Allendorf, C. A. Bauer, R. K. Bhakta and R. J. T. Houk, *Chem. Soc. Rev.*, 2009, **38**, 1330-1352; (c) J. Rocha, F. A. A. Paz, F. N. Shi, R. A. S. Ferreira, T. Trindade and L. D. Carlos, *Eur. J. Inorg. Chem.*, 2009, 4931-4945.
9. (a) B. Joarder, A. K. Chaudhari, S. S. Nagarkar, B. Manna and S. K. Ghosh, *Chem.-Eur. J.*, 2013, **19**, 11178-11183; (b) T. T. Luo, L. Y. Hsu, C. C. Su, C. H. Ueng, T. C. Tsai and K. L. Lu, *Inorg. Chem.*, 2007, **46**, 1532-1534.
10. (a) A. D. Naik, M. M. Dirtu, A. P. Railliet, J. Marchand-Brynaert and Y. Garcia, *Polymers*, 2011, **3**, 1750-1775; (b) C. Li, K. Deng, Z. Y. Tang and L. Jiang, *J. Am. Chem. Soc.*, 2010, **132**, 8202-8209.
11. T. Kundu, S. C. Sahoo and R. Banerjee, *Cryst. Growth Des.*, 2012, **12**, 4633-4640.
12. (a) J. A. Gould, J. T. A. Jones, J. Bacsá, Y. Z. Khimiyak and M. J. Rosseinsky, *Chem. Commun.*, 2010, **46**, 2793-2795; (b) I. Imaz, M. Rubio-Martinez, W. J. Saletta, D. B. Amabilino and D. Maspoch, *J. Am. Chem. Soc.*, 2009, **131**, 18222-18223; (c) R. Vaidhyanathan, D. Bradshaw, J. N. Rebilly, J. P. Barrio, J. A. Gould, N. G. Berry and M. J. Rosseinsky, *Angew. Chem., Int. Ed.*, 2006, **45**, 6495-6499; (d) E. V. Anokhina, Y. B. Go, Y. Lee, T. Vogt and A. J. Jacobson, *J. Am. Chem. Soc.*, 2006, **128**, 9957-9962; (e) E. V. Anokhina and A. J. Jacobson, *J. Am. Chem. Soc.*, 2004, **126**, 3044-3045.
13. J. J. Zhang, T. L. Sheng, S. M. Hu, S. Q. Xia, G. Leibelng, F. Meyer, Z. Y. Fu, L. Chen, R. B. Fu and X. T. Wu, *Chem.-Eur. J.*, 2004, **10**, 3963-3969.
14. M. J. Ingleson, J. Bacsá and M. J. Rosseinsky, *Chem. Commun.*, 2007, 3036-3038.
15. J. K. Maclaren and C. Janiak, *Inorg. Chim. Acta*, 2012, **389**, 183-190.
16. Y. G. Zhang, M. K. Saha and I. Bernal, *CrystEngComm*, 2003, **5**, 34-37.

17. (a) J. H. He, G. J. Zhang, D. R. Xiao, H. Y. Chen, S. W. Yan, X. Wang, J. Yang and E. B. Wang, *CrystEngComm*, 2012, **14**, 3609-3614; (b) L. Chen and X. H. Bu, *Chem. Mater.*, 2006, **18**, 1857-1860.
18. L. J. Dong, W. Chu, Q. L. Zhu and R. D. Huang, *Cryst. Growth Des.*, 2011, **11**, 93-99.
19. I. Imaz, M. Rubio-Martinez, J. An, I. Sole-Font, N. L. Rosi and D. Maspoch, *Chem. Commun.*, 2011, **47**, 7287-7302.
20. J. A. Gould, J. Bacsa, H. Park, J. B. Claridge, A. M. Fogg, V. Ramanathan, J. E. Warren and M. J. Rosseinsky, *Cryst. Growth Des.*, 2010, **10**, 2977-2982.
21. J. P. Barrio, J. N. Rebilly, B. Carter, D. Bradshaw, J. Bacsa, A. Y. Ganin, H. Park, A. Trewin, R. Vaidhyanathan, A. I. Cooper, J. E. Warren and M. J. Rosseinsky, *Chem.-Eur. J.*, 2008, **14**, 4521-4532.
22. T. Kundu, S. C. Sahoo and R. Banerjee, *CrystEngComm*, 2013, **15**, 9634-9640.
23. X. L. Yang, M. H. Xie, C. Zou and C. D. Wu, *CrystEngComm*, 2011, **13**, 6422-6430.
24. (a) S. H. Wang, F. K. Zheng, M. F. Wu, Z. F. Liu, J. Chen, G. C. Guo and A. Q. Wu, *CrystEngComm*, 2013, **15**, 2616-2623; (b) Z. R. Qu, H. Zhao, X. S. Wang, Y. H. Li, Y. M. Song, Y. J. Liu, Q. O. Ye, R. G. Xiong, B. F. Abrahams, Z. L. Xue and X. Z. You, *Inorg. Chem.*, 2003, **42**, 7710-7712.
25. (a) Y. M. Shen and J. F. Bai, *Chem. Commun.*, 2010, **46**, 1308-1310; (b) S. N. Wang, H. Xing, Y. Z. Li, J. F. Bai, M. Scheer, Y. Pan and X. Z. You, *Chem. Commun.*, 2007, 2293-2295; (c) S. N. Wang, J. F. Bai, Y. Z. Li, Y. Pan, M. Scheer and X. Z. You, *CrystEngComm*, 2007, **9**, 1084-1095; (d) S. Wang, J. F. Bai, H. Xing, Y. Z. Li, Y. Song, Y. Pan, M. Scheer and X. Z. You, *Cryst. Growth Des.*, 2007, **7**, 747-754.
26. (a) S. M. F. Vilela, J. A. Fernandes, D. Ananias, L. D. Carlos, J. Rocha, J. P. C. Tomé and F. A. A. Paz, *CrystEngComm*, 2014, **16**, 344-358; (b) B. Monteiro, J. A. Fernandes, C. C. L. Pereira, S. M. F. Vilela, J. P. C. Tome, J. Marcalo and F. A. A. Paz, *Acta Cryst. B*, 2014, **70**, 28-36; (c) S. M. F. Vilela, R. F. Mendes, P. Silva, J. A. Fernandes, J. P. C. Tomé and F. A. A. Paz, *Cryst. Growth Des.*, 2013, **13**, 543-560; (d) S. M. F. Vilela, A. D. G. Firmino, R. F. Mendes, J. A. Fernandes, D. Ananias, A. A. Valente, H. Ott, L. D. Carlos, J. Rocha, J. P. C. Tomé and F. A. A. Paz, *Chem. Commun.*, 2013, **49**, 6400-6402; (e) P. Silva, L. Cunha-Silva, N. J. O. Silva, J. Rocha and F. A. A. Paz, *Cryst. Growth Des.*, 2013, **13**, 2607-2617; (f) F. N. Shi, F. A. A. Paz, P. Ribeiro-Claro and J.

- Rocha, *Chem. Commun.*, 2013, **49**, 11668-11670; (g) S. M. F. Vilela, D. Ananias, A. C. Gomes, A. A. Valente, L. D. Carlos, J. A. S. Cavaleiro, J. Rocha, J. P. C. Tomé and F. A. A. Paz, *J. Mater. Chem.*, 2012, **22**, 18354-18371; (h) F. A. A. Paz, J. Klinowski, S. M. F. Vilela, J. P. C. Tomé, J. A. S. Cavaleiro and J. Rocha, *Chem. Soc. Rev.*, 2012, **41**, 1088-1110; (i) C. B. Liu, R. A. S. Ferreira, F. A. A. Paz, A. Cadiou, L. D. Carlos, L. S. Fu, J. Rocha and F. N. Shi, *Chem. Commun.*, 2012, **48**, 7964-7966; (j) P. Silva, F. Vieira, A. C. Gomes, D. Ananias, J. A. Fernandes, S. M. Bruno, R. Soares, A. A. Valente, J. Rocha and F. A. A. Paz, *J. Am. Chem. Soc.*, 2011, **133**, 15120-15138.
27. S. M. F. Vilela, D. Ananias, J. A. Fernandes, P. Silva, A. C. Gomes, N. J. O. Silva, M. O. Rodrigues, J. P. C. Tomé, A. A. Valente, P. Ribeiro-Claro, L. D. Carlos, J. Rocha and F. A. A. Paz, *J. Mater. Chem. C*, 2014, DOI: 10.1039/c40333tc32114b.
28. (a) F. Gutierrez, C. Tedeschi, L. Maron, J. P. Daudey, R. Poteau, J. Azema, P. Tisnes and C. Picard, *Dalton Trans.*, 2004, 1334-1347; (b) D. Guillaumont, H. Bazin, J. M. Benech, M. Boyer and G. Mathis, *ChemPhysChem*, 2007, **8**, 480-488; (c) C. R. De Silva, J. Li, Z. P. Zheng and L. R. Corrales, *J. Phys. Chem. A*, 2008, **112**, 4527-4530; (d) A. D'Aleo, A. Picot, A. Beeby, J. A. G. Williams, B. Le Guennic, C. Andraud and O. Maury, *Inorg. Chem.*, 2008, **47**, 10258-10268; (e) X. N. Li, Z. J. Wu, Z. J. Si, Z. Liang, X. J. Liu and H. J. Zhang, *Phys. Chem. Chem. Phys.*, 2009, **11**, 9687-9695; (f) M. M. Nolasco, P. D. Vaz and L. D. Carlos, *New J. Chem.*, 2011, **35**, 2435-2441; (g) P. P. Lima, M. M. Nolasco, F. A. A. Paz, R. A. S. Ferreira, R. L. Longo, O. L. Malta and L. D. Carlos, *Chem. Mater.*, 2013, **25**, 586-598; (h) M. M. Nolasco, P. M. Vaz, V. T. Freitas, P. P. Lima, P. S. André, R. A. S. Ferreira, P. D. Vaz, P. Ribeiro-Claro and L. D. Carlos, *J. Mater. Chem. A*, 2013, **1**, 7339-7350.
29. T. Kottke and D. Stalke, *J. App. Cryst.*, 1993, **26**, 615-619.
30. APEX2, *Data Collection Software Version 2.1-RC13*, Bruker AXS, Delft, The Netherlands, 2006.
31. Cryopad, *Remote monitoring and control, Version 1.451*, Oxford Cryosystems, Oxford, United Kingdom, 2006.
32. SAINT+, *Data Integration Engine v. 7.23a* ©, 1997-2005, **Bruker AXS, Madison, Wisconsin, USA**.
33. G. M. Sheldrick, *SADABS v.2.01*, Bruker/Siemens Area Detector Absorption Correction Program, 1998, **Bruker AXS, Madison, Wisconsin, USA**.

34. (a) G. M. Sheldrick, *SHELXS-97, Program for Crystal Structure Solution, University of Göttingen*, 1997; (b) G. M. Sheldrick, *Acta Cryst. A*, 2008, **64**, 112-122.
35. G. M. Sheldrick, *SHELXL-97, Program for Crystal Structure Refinement, University of Göttingen*, 1997.
36. K. Brandenburg, *DIAMOND, Version 3.2, Crystal Impact GbR, Bonn, Germany*, 2006.
37. (a) C. T. Lee, W. T. Yang and R. G. Parr, *Phys. Rev. B*, 1988, **37**, 785-789; (b) A. D. Becke, *J. Chem. Phys.*, 1993, **98**, 5648-5652.
38. M. Dolg, H. Stoll, A. Savin and H. Preuss, *Theor. Chim. Acta*, 1989, **75**, 173-194.
39. R. E. Stratmann, G. E. Scuseria and M. J. Frisch, *J. Chem. Phys.*, 1998, **109**, 8218-8224.
40. M. J. Frisch, G. W. Trucks, H. B. Schlegel, G. E. Scuseria, M. A. Robb, J. R. Cheeseman, G. Scalmani, V. Barone, B. Mennucci, G. A. Petersson, H. Nakatsuji, M. Caricato, X. Li, H. P. Hratchian, A. F. Izmaylov, J. Bloino, G. Zheng, J. L. Sonnenberg, M. Hada, M. Ehara, K. Toyota, R. Fukuda, J. Hasegawa, M. Ishida, T. Nakajima, Y. Honda, O. Kitao, H. Nakai, T. Vreven, J. A. Montgomery, Jr., J. E. Peralta, F. Ogliaro, M. Bearpark, J. J. Heyd, E. Brothers, K. N. Kudin, V. N. Staroverov, R. Kobayashi, J. Normand, K. Raghavachari, A. Rendell, J. C. Burant, S. S. Iyengar, J. Tomasi, M. Cossi, N. Rega, N. J. Millam, M. Klene, J. E. Knox, J. B. Cross, V. Bakken, C. Adamo, J. Jaramillo, R. Gomperts, R. E. Stratmann, O. Yazyev, A. J. Austin, R. Cammi, C. Pomelli, J. W. Ochterski, R. L. Martin, K. Morokuma, V. G. Zakrzewski, G. A. Voth, P. Salvador, J. J. Dannenberg, S. Dapprich, A. D. Daniels, Ö. Farkas, J. B. Foresman, J. V. Ortiz, J. Cioslowski and D. J. Fox, *Gaussian 09, Revision A.02. Gaussian, Inc., Wallingford CT*, 2009.
41. *U. S. Patent 4,402,907 Pat.*, 1983.
42. S. M. F. Vilela, F. A. A. Paz, J. P. C. Tomé, V. D. Bermudez, J. A. S. Cavaleiro and J. Rocha, *Acta Cryst. E*, 2009, **65**, O1970-U3925.
43. (a) S. M. F. Vilela, F. A. A. Paz, J. P. C. Tomé, V. D. Bermudez, J. A. S. Cavaleiro and J. Rocha, *Acta Cryst. E*, 2009, **65**, O1985-U4085; (b) S. M. F. Vilela, F. A. A. Paz, J. P. C. Tomé, V. D. Bermudez, J. A. S. Cavaleiro and J. Rocha, *Acta Cryst. E*, 2010, **66**, o3243-o3244.
44. (a) F. A. A. Paz and J. Klinowski, *CrystEngComm*, 2003, **5**, 238-244; (b) F. A. A. Paz, A. D. Bond, Y. Z. Khimiyak and J. Klinowski, *New J. Chem.*, 2002, **26**, 381-383.

45. (a) J. Grell, J. Bernstein and G. Tinhofer, *Acta Cryst. B*, 1999, **55**, 1030-1043; (b) J. Bernstein, R. E. Davis, L. Shimoni and N. L. Chang, *Angew. Chem. Int. Edit. Engl.*, 1995, **34**, 1555-1573.
46. (a) F. H. Allen and W. D. S. Motherwell, *Acta Cryst. B*, 2002, **58**, 407-422; (b) F. H. Allen, *Acta Cryst. B*, 2002, **58**, 380-388.
47. G. Socrates, *Infrared Characteristic Group Frequencies: Tables and Charts*, 2<sup>nd</sup> edn., John Wiley & Sons Ltd, Baffins Lane, Chichester, 1994.
48. (a) D. C. Oliveira, A. G. Macedo, N. J. O. Silva, C. Molina, R. A. S. Ferreira, P. S. André, K. Dahmouche, V. D. Bermudez, Y. Messaddeq, S. J. L. Ribeiro and L. D. Carlos, *Chem. Mater.*, 2008, **20**, 3696-3705; (b) M. Nara and M. Tanokura, *Biochem. Biophys. Res. Commun.*, 2008, **369**, 225-239; (c) Y. Sorek, M. Zevin, R. Reisfeld, T. Hurvits and S. Ruschin, *Chem. Mater.*, 1997, **9**, 670-676.
49. D. Ananias, M. Kostova, F. A. A. Paz, A. Ferreira, L. D. Carlos, J. Klinowski and J. Rocha, *J. Am. Chem. Soc.*, 2004, **126**, 10410-10417.
50. (a) G. I. Romanovskaya, *J. Anal. Chem.*, 2009, **64**, 755-760; (b) J. S. de Klerk, A. Szemik-Hojniak, F. Ariese and C. Gooijer, *Spectrochim. Acta, Part A*, 2009, **72**, 144-150.
51. L. D. C. Baldi and T. D. Z. Atvars, *Polímeros*, 2005, **15**, 33-38.
52. J. S. de Klerk, A. N. Bader, S. Zapotoczny, M. Sterzel, M. Pilch, A. Danel, C. Gooijer and F. Ariese, *J. Phys. Chem. A*, 2009, **113**, 5273-5279.
53. A. N. Bader, F. Ariese and C. Gooijer, *J. Phys. Chem. A*, 2002, **106**, 2844-2849.
54. (a) K. Jayaramulu, P. Kanoo, S. J. George and T. K. Maji, *Chem. Commun.*, 2010, **46**, 7906-7908; (b) K. Jayaramulu, R. P. Narayanan, S. J. George and T. K. Maji, *Inorg. Chem.*, 2012, **51**, 10089-10091.
55. K.-L. Han and G.-J. Zhao, *Hydrogen Bonding and Transfer in the Excited State*, John Wiley & Sons, 2010.
56. J. M. Oliva, E. Azenha, H. D. Burrows, R. Coimbra, J. S. S. de Melo, M. L. Canle, M. I. Fernandez, J. A. Santaballa and L. Serrano-Andres, *ChemPhysChem*, 2005, **6**, 306-314.

## Table 1

**Table 1.** Crystal and structure refinement data for  $L'$ ,  $H_2bodt \cdot HCl$  and  $[La(bodt)(Hbodt)]$  (**1**).

	$L'$	$H_2bodt \cdot HCl$	<b>1</b>
Formula	$C_9H_{12}ClN_5O_4$	$C_7H_{10}ClN_5O_5$	$C_{14}H_{15}LaN_{10}O_{10}$
Formula weight	289.69	279.65	622.27
Temperature / K	150(2)	150(2)	150(2)
Crystal system	Monoclinic	Monoclinic	Monoclinic
Space group	$P2_1/n$	$P2_1/c$	$P2/c$
$a / \text{Å}$	7.2191(5)	11.2216(3)	13.013(2)
$b / \text{Å}$	24.9432(19)	15.0063(4)	8.7755(16)
$c / \text{Å}$	7.4918(5)	6.8432(2)	8.4187(13)
$\alpha / ^\circ$	90	90	90
$\beta / ^\circ$	113.281(5)	90.245(2)	103.902(5)
$\gamma / ^\circ$	90	90	90
Volume/ $\text{Å}^3$	1239.19(15)	1152.35(6)	933.2(3)
$Z$	4	4	1
$D_c/\text{g cm}^{-3}$	1.553	1.612	2.214
$\mu(\text{Mo-K}\alpha)/\text{mm}^{-1}$	0.328	0.356	2.377
Crystal size/mm	0.26×0.20×0.18	0.10×0.08×0.02	0.04×0.02×0.01
Crystal type	Colorless prism	Colorless plate	Colorless plate
$\theta$ range	3.70 to 27.48	3.63 to 36.31	3.98 to 27.47
Index ranges	$-9 \leq h \leq 9$ $-31 \leq k \leq 28$ $-9 \leq l \leq 9$	$-18 \leq h \leq 15$ $-25 \leq k \leq 23$ $-11 \leq l \leq 11$	$-16 \leq h \leq 16$ $-10 \leq k \leq 11$ $-6 \leq l \leq 10$
Reflections collected	13354	20434	8544
Independent reflections	2810 ( $R_{\text{int}} = 0.0682$ )	5566 ( $R_{\text{int}} = 0.0314$ )	2112 ( $R_{\text{int}} = 0.0995$ )
Data completeness	up to $\theta = 27.48^\circ$ 98.7%	up to $\theta = 36.31^\circ$ 99.4%	up to $\theta = 27.47^\circ$ 98.6%
Data / parameters	2810 / 180	5566 / 165	2112 / 159
Final $R$ indices	$R1 = 0.0476$	$R1 = 0.0398$	$R1 = 0.0454$
$[I > 2\sigma(I)]^{a,b}$	$wR2 = 0.1101$	$wR2 = 0.0943$	$wR2 = 0.0690$
Final $R$ indices (all data) <sup>a,b</sup>	$R1 = 0.0835$ $wR2 = 0.1275$	$R1 = 0.0657$ $wR2 = 0.1056$	$R1 = 0.0766$ $wR2 = 0.0766$
Largest diff. peak and hole	0.576 and $-0.382 \text{ e} \cdot \text{Å}^{-3}$	0.469 and $-0.254 \text{ e} \cdot \text{Å}^{-3}$	1.110 and $-1.202 \text{ e} \cdot \text{Å}^{-3}$

$$^a R1 = \sum ||F_o| - |F_c|| / \sum |F_o|; \quad ^b wR2 = \sqrt{\sum [w(F_o^2 - F_c^2)^2] / \sum [w(F_o^2)^2]}$$

## Table 2

**Table 2.** Hydrogen bonding geometry (distances in Å and angles in degrees) for the intermediate compound **L'**.<sup>a</sup>

D–H···A	<i>d</i> (D···A)	<(DHA)
N4–H4···N1 <sup>i</sup>	2.6291(12)	177
N5–H5···N2 <sup>ii</sup>	2.6337(12)	177

<sup>a</sup> Symmetry transformations used to generate equivalent atoms:

(i)  $2-x, 2-y, 1-z$ ; (ii)  $1-x, 2-y, 2-z$ .

## Table 3

**Table 3.** Hydrogen bonding geometry (distances in Å and angles in degrees) for the supramolecular salt H<sub>2</sub>bodt·HCl.<sup>a</sup>

D–H···A	<i>d</i> (D···A)	<(DHA)
O3–H3···O4 <sup>i</sup>	2.6291(12)	177
O5–H5A···O2 <sup>i</sup>	2.6337(12)	177
N1–H1···C11 <sup>ii</sup>	3.0735(9)	157
N2–H2···C11 <sup>iii</sup>	3.1863(9)	153
N4–H4···C11 <sup>iii</sup>	3.1817(10)	155
N5–H5···C11 <sup>ii</sup>	3.3430(9)	145

<sup>a</sup> Symmetry transformations used to generate equivalent atoms:

(i)  $1-x, -y, -z$ ; (ii)  $x, \frac{1}{2}-y, -\frac{1}{2}+z$ ; (iii)  $-x, -y, 1-z$ .

## Table 4

**Table 4.** Selected bond distances (in Å) and angles (in degrees) for the La<sup>3+</sup> coordination environments present in [La(bodt)(Hbodt)] (1).<sup>a</sup>

La1–O1	2.688(3)	La1–O3 <sup>iii</sup>	2.660(3)
La1–O1 <sup>iii</sup>	2.688(3)	La1–O4	2.713(3)
La1–O2	2.549(3)	La1–O4 <sup>i</sup>	2.528(3)
La1–O2 <sup>iii</sup>	2.549(3)	La1–O4 <sup>ii</sup>	2.528(3)
La1–O3	2.660(3)	La1–O4 <sup>iii</sup>	2.713(3)
O1–La1–O1 <sup>iii</sup>	143.52(16)	O3 <sup>iii</sup> –La1–O4	108.08(11)
O1–La1–O4	93.99(10)	O3 <sup>iii</sup> –La1–O4 <sup>iii</sup>	48.32(10)
O1–La1–O4 <sup>iii</sup>	78.46(10)	O3–La1–O4	48.32(10)
O1 <sup>iii</sup> –La1–O4	78.46(10)	O3–La1–O4 <sup>iii</sup>	108.08(11)
O1 <sup>iii</sup> –La1–O4 <sup>iii</sup>	93.99(10)	O4 <sup>i</sup> –La1–O2	72.67(11)
O2–La1–O1	49.78(11)	O4 <sup>ii</sup> –La1–O2	77.36(11)
O2–La1–O1 <sup>iii</sup>	148.93(10)	O4 <sup>i</sup> –La1–O1	122.46(11)
O2 <sup>iii</sup> –La1–O1	148.93(10)	O4 <sup>i</sup> –La1–O1 <sup>iii</sup>	86.76(10)
O2 <sup>iii</sup> –La1–O2	140.64(17)	O4 <sup>ii</sup> –La1–O1	86.76(10)
O2–La1–O3	87.02(11)	O4 <sup>ii</sup> –La1–O1 <sup>iii</sup>	122.46(11)
O2–La1–O3 <sup>iii</sup>	128.66(11)	O4 <sup>i</sup> –La1–O2 <sup>iii</sup>	77.36(11)
O2 <sup>iii</sup> –La1–O3	128.66(11)	O4 <sup>i</sup> –La1–O3	113.04(10)
O2 <sup>iii</sup> –La1–O3 <sup>iii</sup>	87.02(11)	O4 <sup>i</sup> –La1–O3 <sup>iii</sup>	155.97(10)
O2–La1–O4	71.81(11)	O4 <sup>ii</sup> –La1–O3	155.97(10)
O2–La1–O4 <sup>iii</sup>	116.91(10)	O4 <sup>ii</sup> –La1–O3 <sup>iii</sup>	113.04(10)
O2 <sup>iii</sup> –La1–O1 <sup>iii</sup>	49.78(11)	O4 <sup>i</sup> –La1–O4	64.74(13)
O2 <sup>iii</sup> –La1–O4	116.91(10)	O4 <sup>ii</sup> –La1–O4	138.29(9)
O2 <sup>iii</sup> –La1–O4 <sup>iii</sup>	71.81(11)	O4 <sup>iii</sup> –La1–O4	155.93(16)
O3–La1–O1	69.22(10)	O4 <sup>i</sup> –La1–O4 <sup>ii</sup>	79.82(15)
O3–La1–O1 <sup>iii</sup>	79.77(11)	O4 <sup>i</sup> –La1–O4 <sup>iii</sup>	138.29(9)
O3–La1–O3 <sup>iii</sup>	63.47(14)	O4 <sup>ii</sup> –La1–O2 <sup>iii</sup>	72.67(11)
O3 <sup>iii</sup> –La1–O1	79.77(11)	O4 <sup>ii</sup> –La1–O4 <sup>iii</sup>	64.74(13)
O3 <sup>iii</sup> –La1–O1 <sup>iii</sup>	69.22(10)		

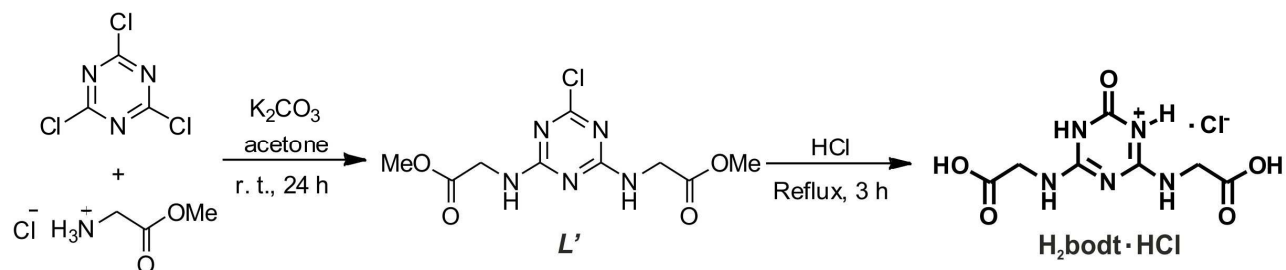
<sup>a</sup> Symmetry transformations used to generate equivalent atoms: (i)  $I-x, 2-y, I-z$ ; (ii)  $x, 2-y, -\frac{1}{2}+z$ ; (iii)  $I-x, y, \frac{1}{2}-z$ .

**Table 5****Table 5.** Hydrogen bonding geometry (distances in Å and angles in degrees) for [La(bodt)(Hbodt)] (**1**).<sup>a</sup>

D–H···A	<i>d</i> (D···A)	<(DHA)
N1–H1···O5 <sup>iv</sup>	2.859(5)	176
N3–H3···O1 <sup>v</sup>	2.821(5)	150
N4–H4···N4 <sup>iv</sup>	2.755(8)	174
N5–H5···O1 <sup>v</sup>	2.970(6)	144

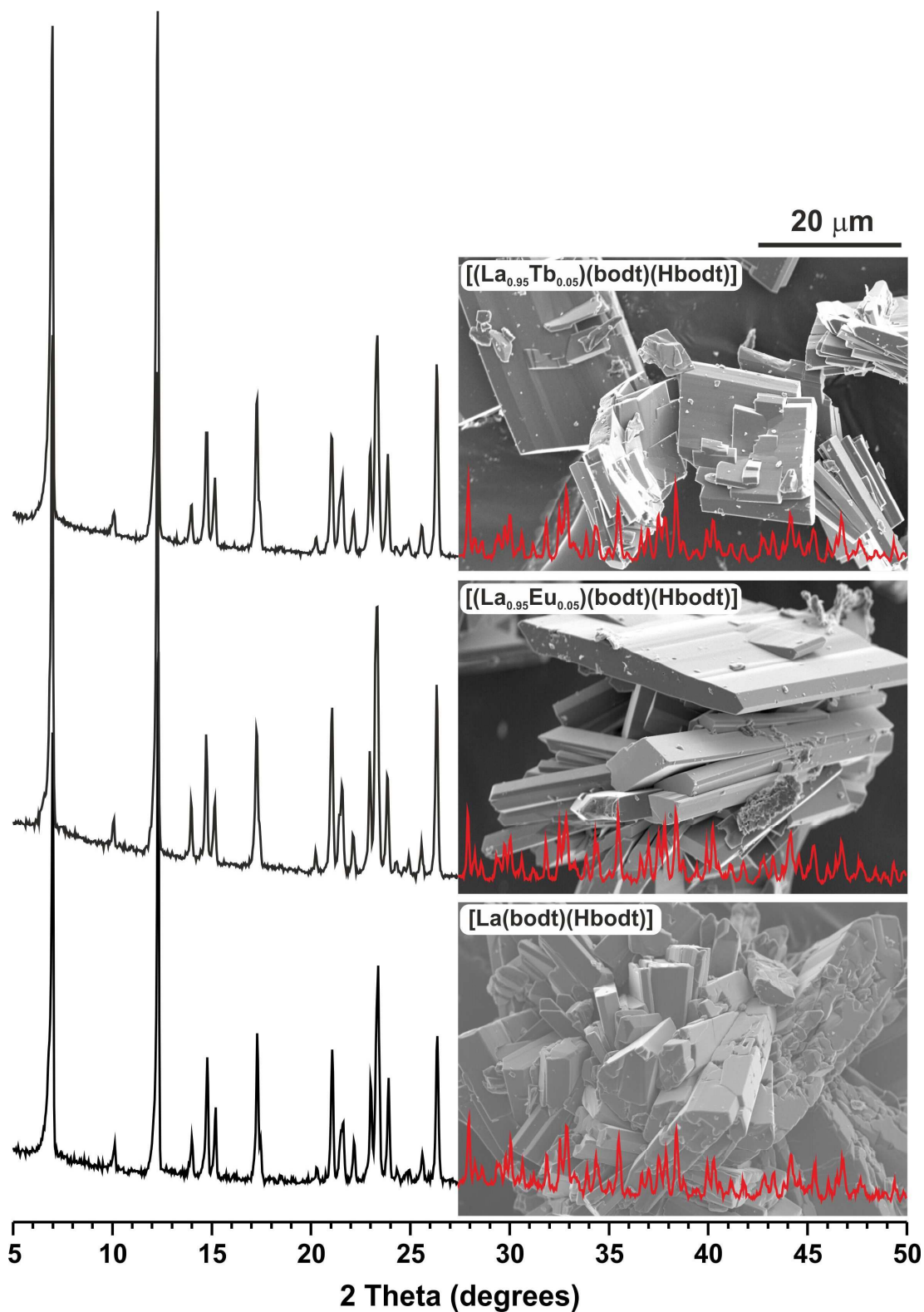
<sup>a</sup> Symmetry transformations used to generate equivalent atoms:  
(iv)  $-x, 1-y, -z$ ; (v)  $x, 1-y, \frac{1}{2}+z$ .

## Scheme 1



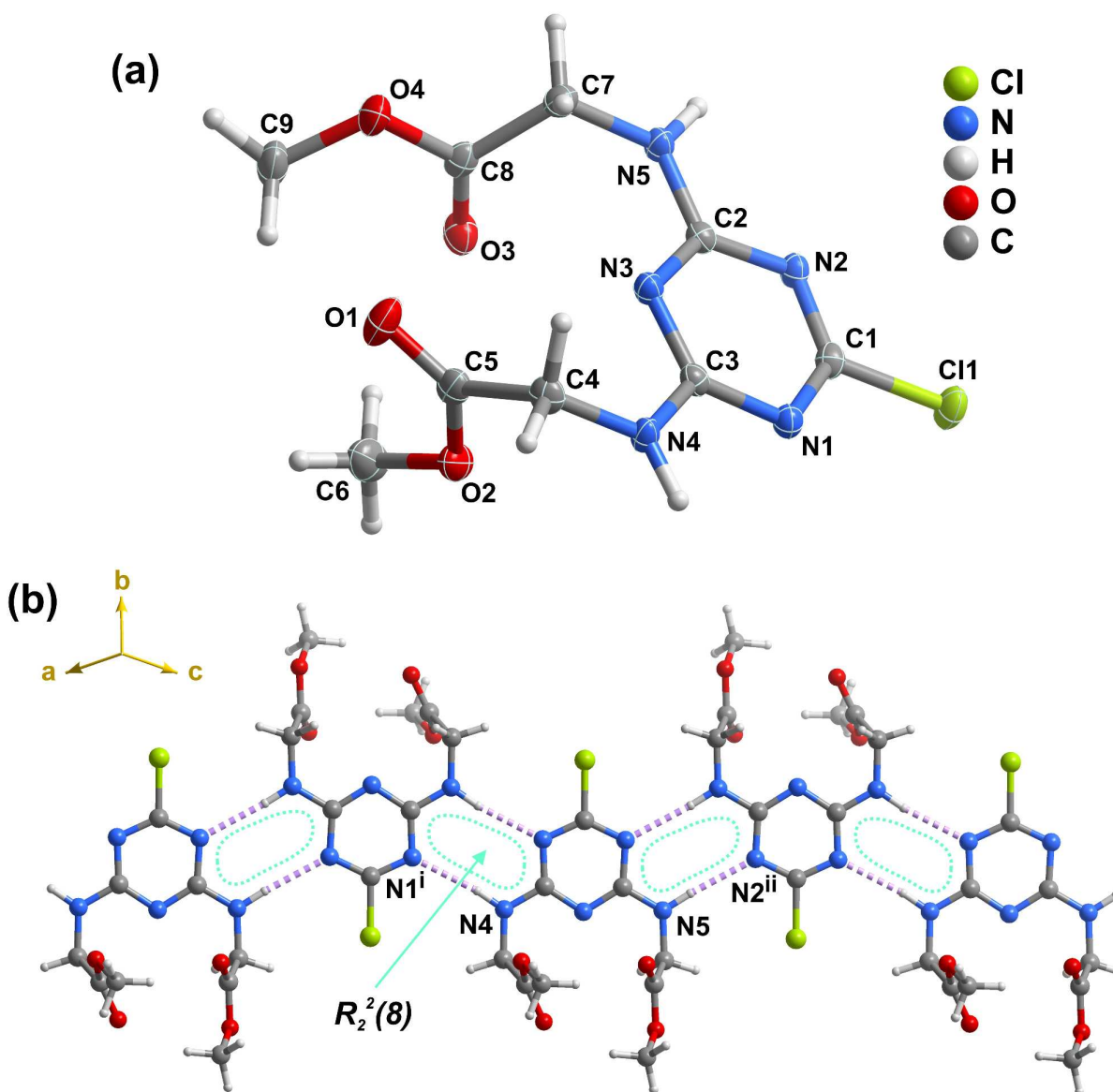
**Scheme 1.** Two-step preparation procedure of the hydrochloric salt 4,6-bis(carboxymethylamino)-2-oxo-2,3-dihydro-1,3,5-triazin-1-ium chloride ( $\text{H}_2\text{bodt}\cdot\text{HCl}$ ) from cyanuric chloride and glycine methyl ester hydrochloride.

# Figure 1



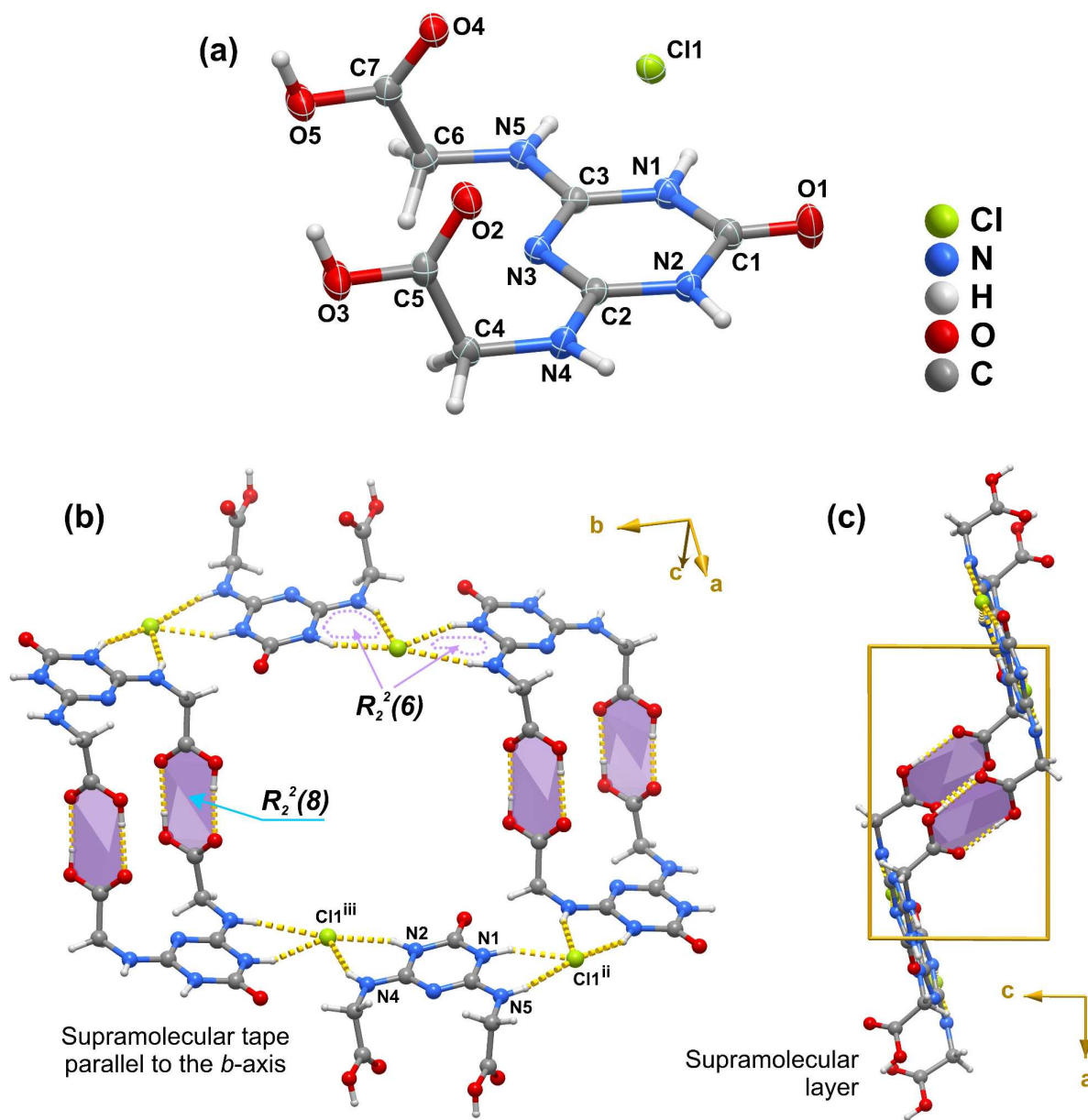
**Fig. 1.** Powder X-ray diffraction and SEM images of bulk  $[Ln(bodt)(Hbodt)]$  materials [where  $Ln^{3+} = La^{3+}$  (1),  $(La_{0.95}Eu_{0.05})$  (2) and  $(La_{0.95}Tb_{0.05})$  (3)] prepared under hydrothermal conditions.

## Figure 2



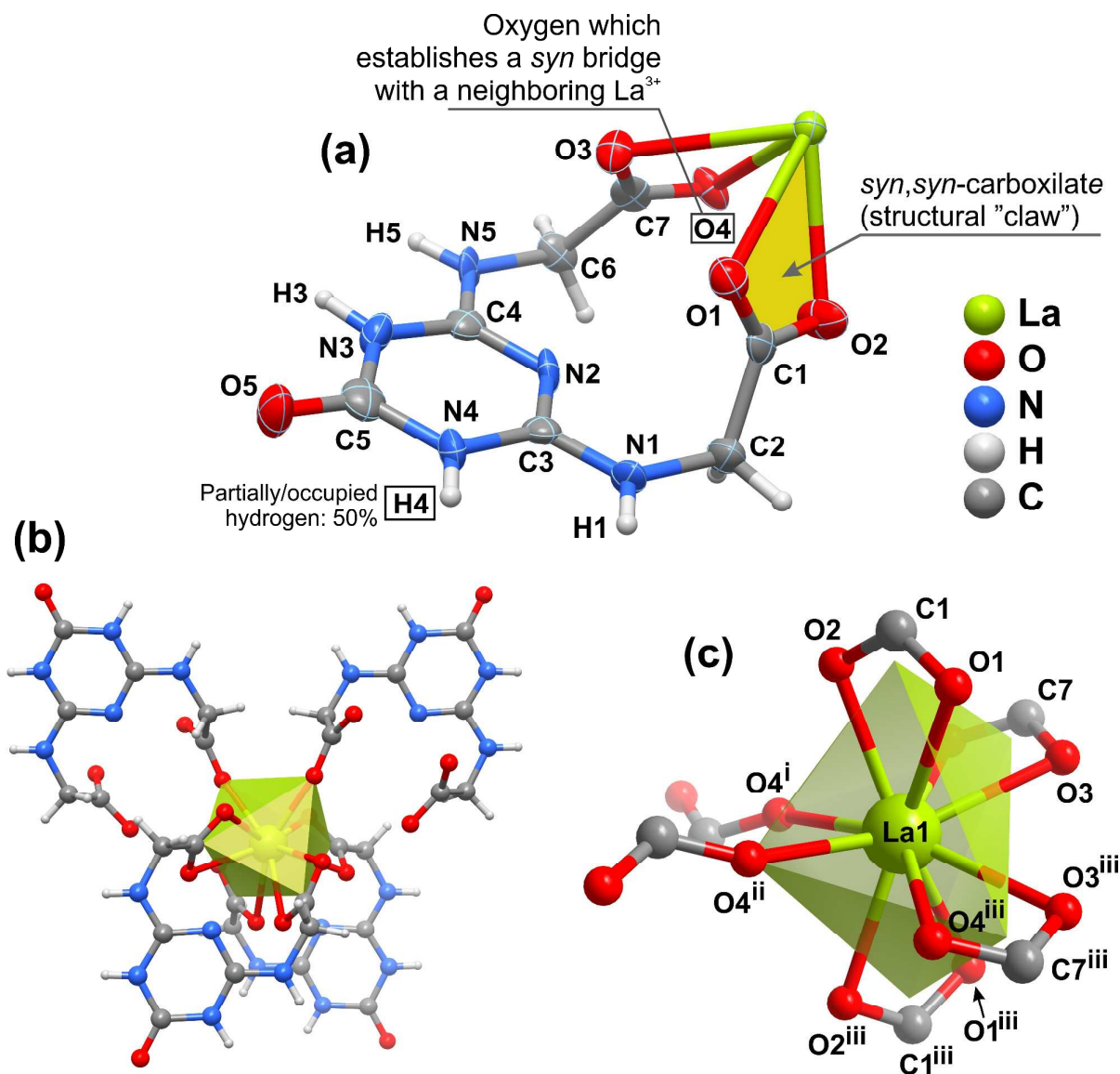
**Fig. 2** (a) Schematic representation of the molecular unit present in the intermediate compound  $L'$ . Non-hydrogen atoms are represented as thermal ellipsoids drawn at the 50% probability level and hydrogen atoms as spheres with arbitrary radii. The atomic labeling scheme is provided for all non-hydrogen atoms. (b) Fragment of the crystal structure of  $L'$  emphasising the cooperative N–H $\cdots$ N hydrogen bonds interconnecting adjacent molecular units via  $R_2^2(8)$  graph set motifs, forming a supramolecular zigzag tape. For geometric details on the represented hydrogen bonding interactions see Table 2. Symmetry transformations used to generate equivalent atoms: (i)  $2-x, 2-y, 1-z$ ; (ii)  $1-x, 2-y, 2-z$ .

## Figure 3

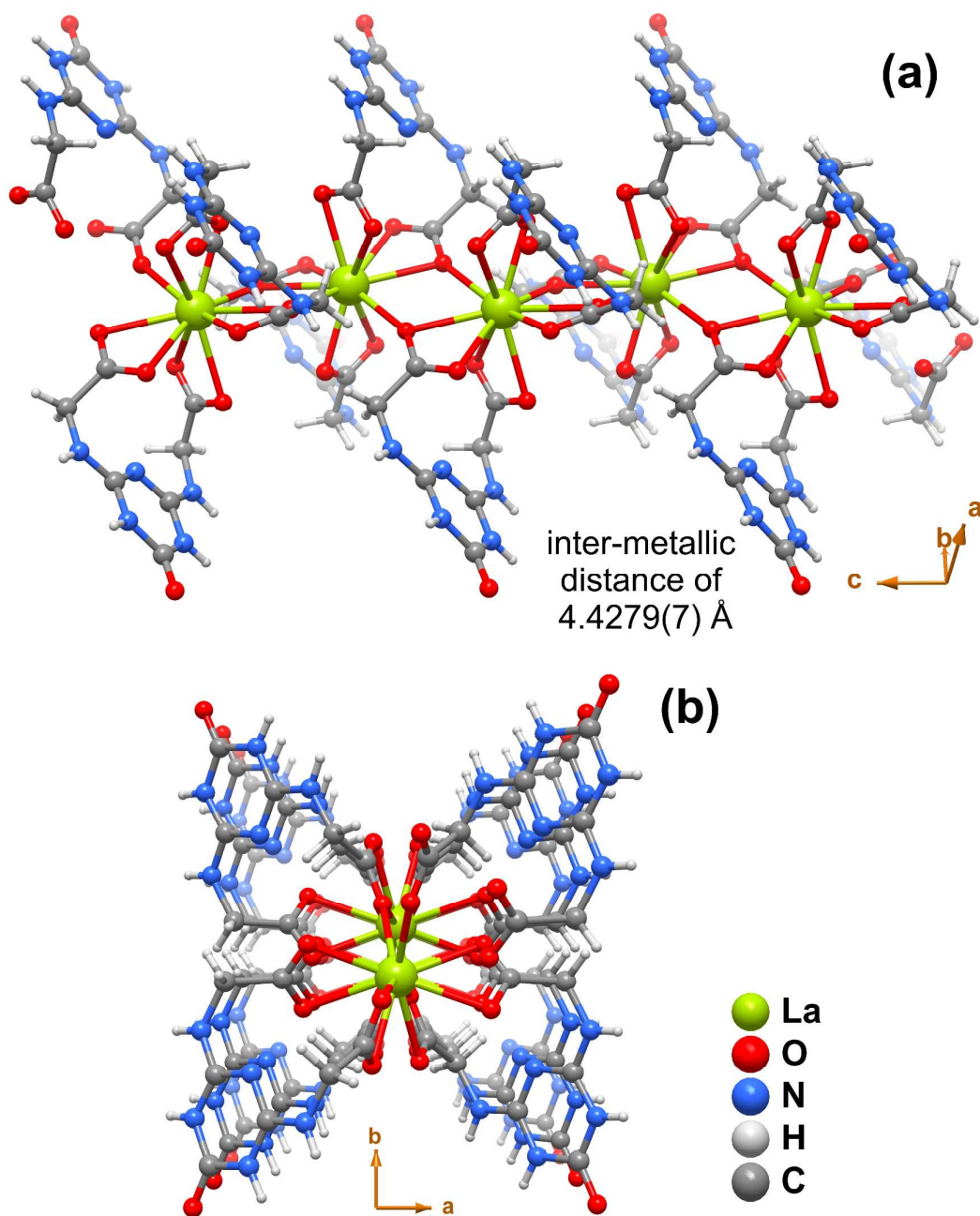


**Fig. 3** (a) Schematic representation of the anionic (chloride anion) and cationic (protonated hydrolysed organic moiety) molecular units present in the supramolecular salt  $\text{H}_2\text{bodt}\cdot\text{HCl}$ . Non-hydrogen atoms are represented as thermal ellipsoids drawn at the 50% probability level and hydrogen atoms as spheres with arbitrary radii. The atomic labeling scheme is provided for all non-hydrogen atoms. (b) Fragment of the crystal structure of  $\text{H}_2\text{bodt}\cdot\text{HCl}$  emphasising the  $\text{O}-\text{H}\cdots\text{O}$  and  $\text{N}-\text{H}\cdots\text{Cl}$  hydrogen bonds interconnecting adjacent chemical entities. For geometric details on the represented hydrogen bonding interactions see Table 3. Symmetry transformations used to generate equivalent atoms: (ii)  $x, \frac{1}{2}-y, -\frac{1}{2}+z$ ; (iii)  $-x, -y, 1-z$ .

## Figure 4

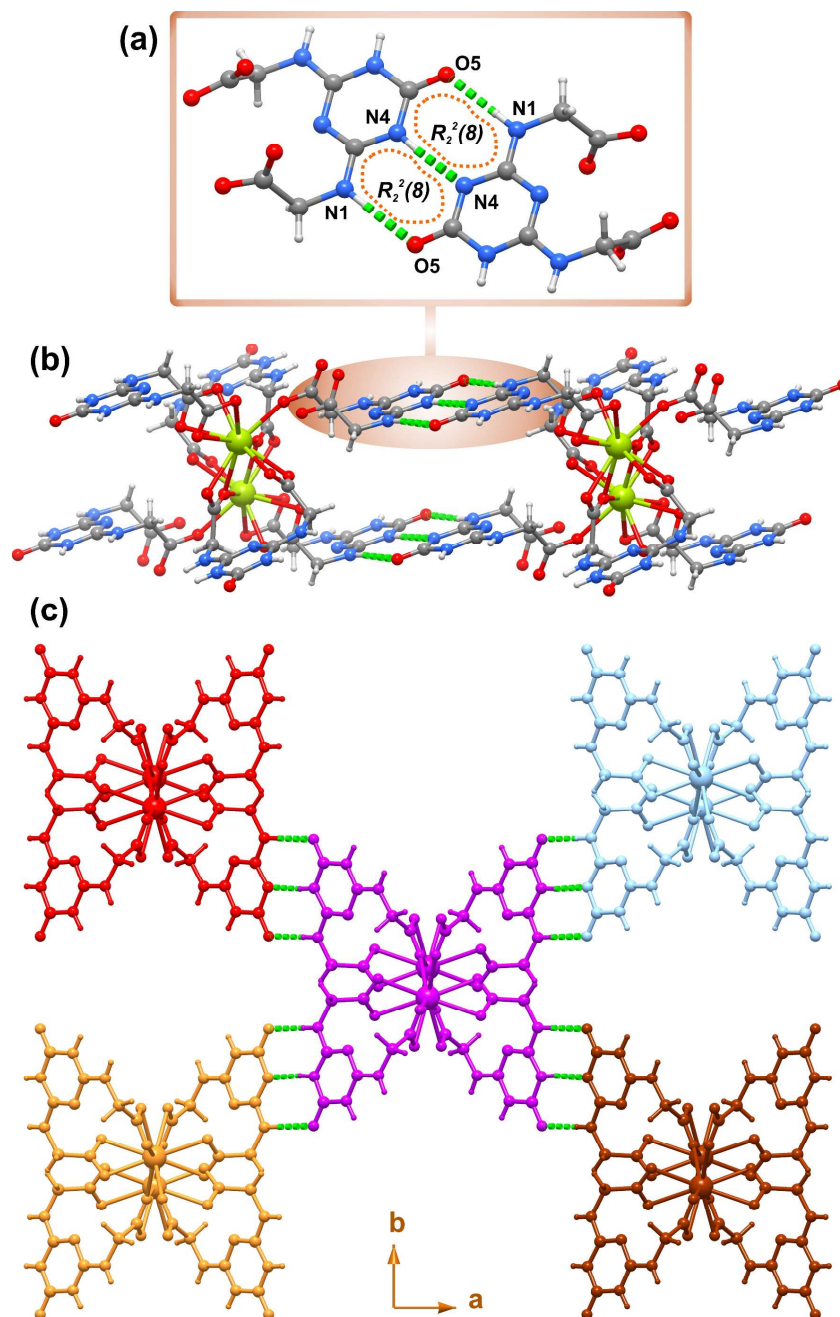


**Fig. 4** (a) Schematic representation of the asymmetric unit of  $[\text{La}(\text{bodt})(\text{Hbodt})]$  (**1**). Non-hydrogen atoms are represented as thermal ellipsoids drawn at the 80% probability level and hydrogen atoms as spheres with arbitrary radii. The atomic labeling scheme is provided for all non-hydrogen atoms and for hydrogen atoms bound to nitrogen. (b) Coordination environment of the crystallographically independent  $\text{La}^{3+}$  metallic centre emphasising the four symmetry-related organic ligands composing the first coordination sphere. (c) Detailed view of the highly distorted octahedral coordination environment of  $\text{La}^{3+}$  when the centres of gravity of the chelated carboxylate groups are considered as the vertices of the polyhedron. For bond lengths and angles see Table 4. Symmetry transformations used to generate equivalent atoms: (i)  $1-x, 2-y, 1-z$ ; (ii)  $x, 2-y, -\frac{1}{2}+z$ ; (iii)  $1-x, y, \frac{1}{2}-z$ .

**Figure 5**

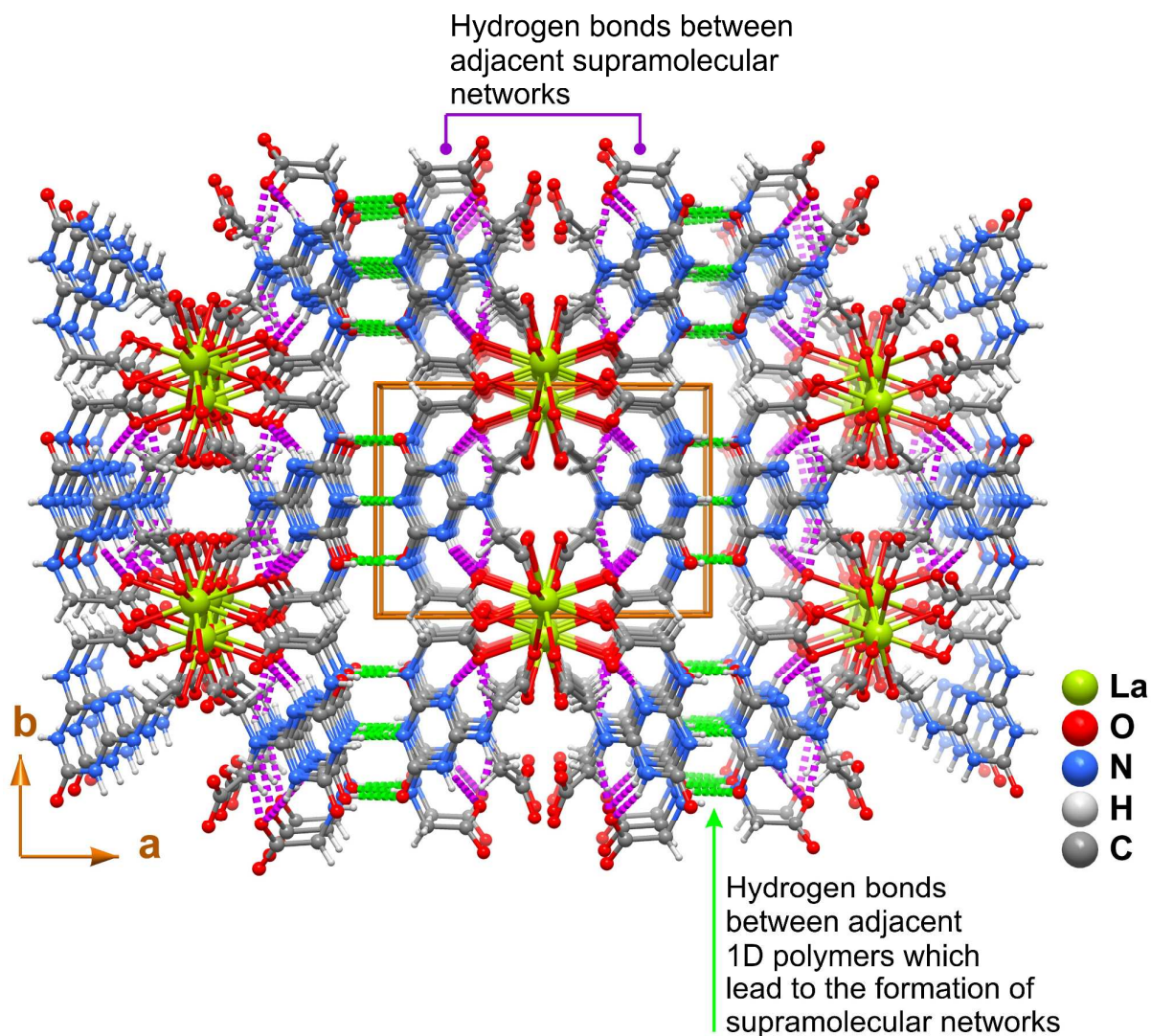
**Fig. 5** Perspective views of the one-dimensional  $\infty^1[\text{La}(\text{bodt})(\text{Hbodt})]$  coordination polymer present in compound **1**.

## Figure 6



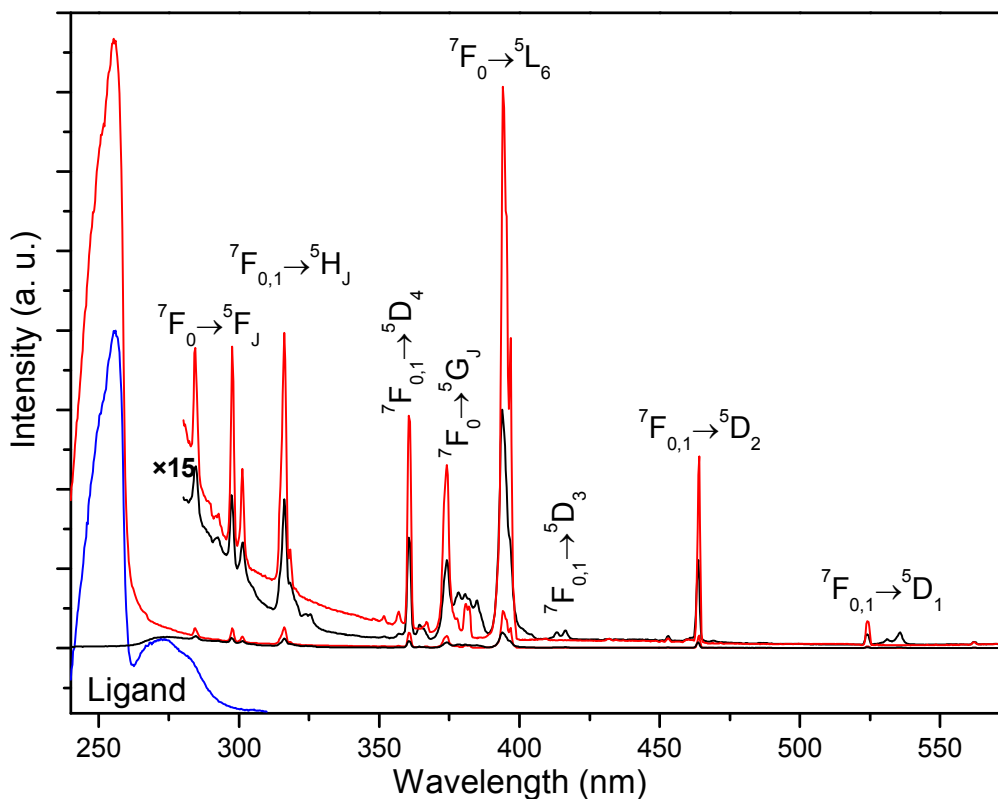
**Fig. 6** Strong supramolecular hydrogen bonding interactions between adjacent  $\infty^1[\text{La}(\text{bodt})(\text{Hbodt})]$  coordination polymers. **(a)** and **(b)** Adjacent  $R_2^2(8)$  graph set motifs connecting neighboring organic rings (*please note*: only one position for the hydrogen atom bound to N4 is represented), which repeat themselves along the [001] direction of the unit cell. **(c)** Hydrogen bonds of one  $\infty^1[\text{La}(\text{bodt})(\text{Hbodt})]$  polymer to four neighbour identical entities, ultimately forming a supramolecular 3D network. For geometric details on the represented hydrogen bonding interactions see Table 5. Symmetry transformations used to generate equivalent atoms have been omitted for clarity.

## Figure 7

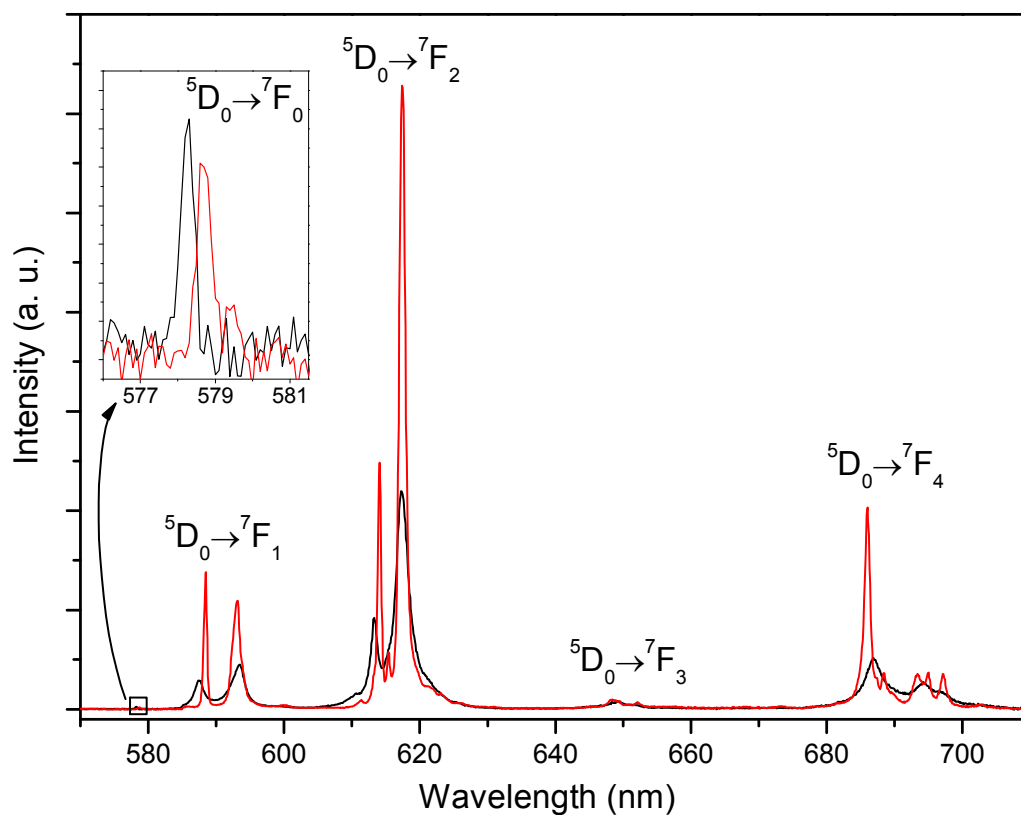


**Fig. 7** Crystal packing of [La(bodt)(Hbodt)] (**1**) viewed in perspective along the [001] direction of the unit cell. N–H···(N,O) hydrogen bonds connecting adjacent 1D polymers are represented as dashed purple lines. N–H···O interactions establishing connections between adjacent supramolecular networks are drawn as dashed green lines. For hydrogen bonding geometric details see Table 5.

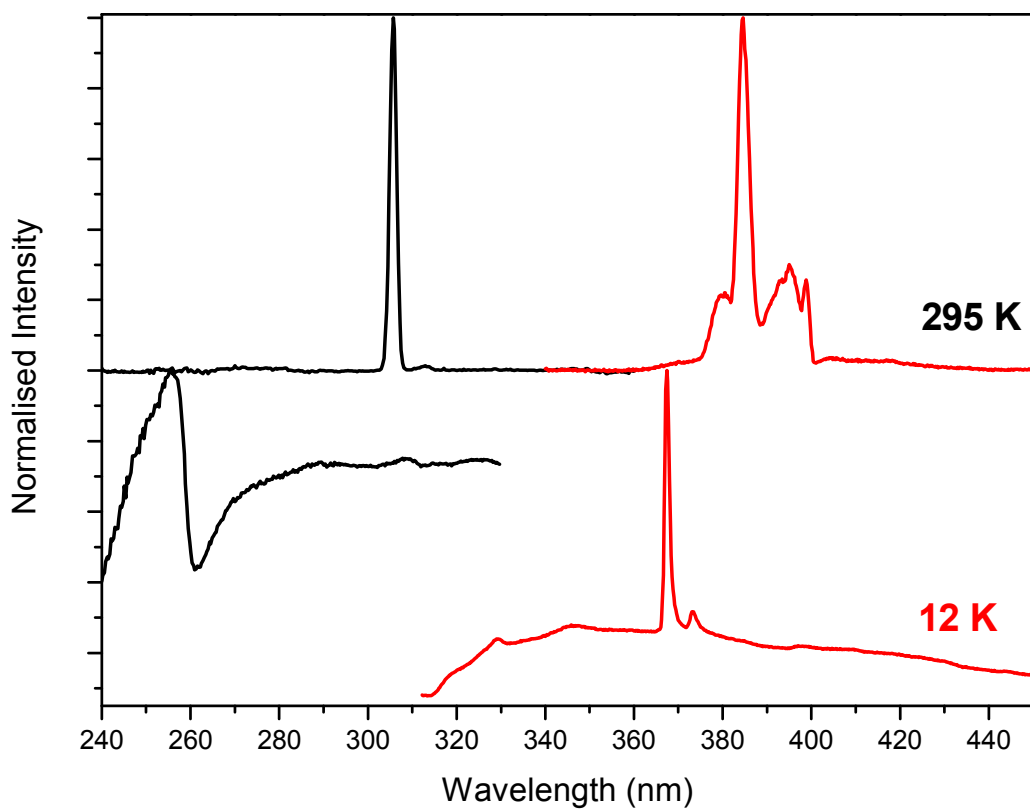
## Figure 8



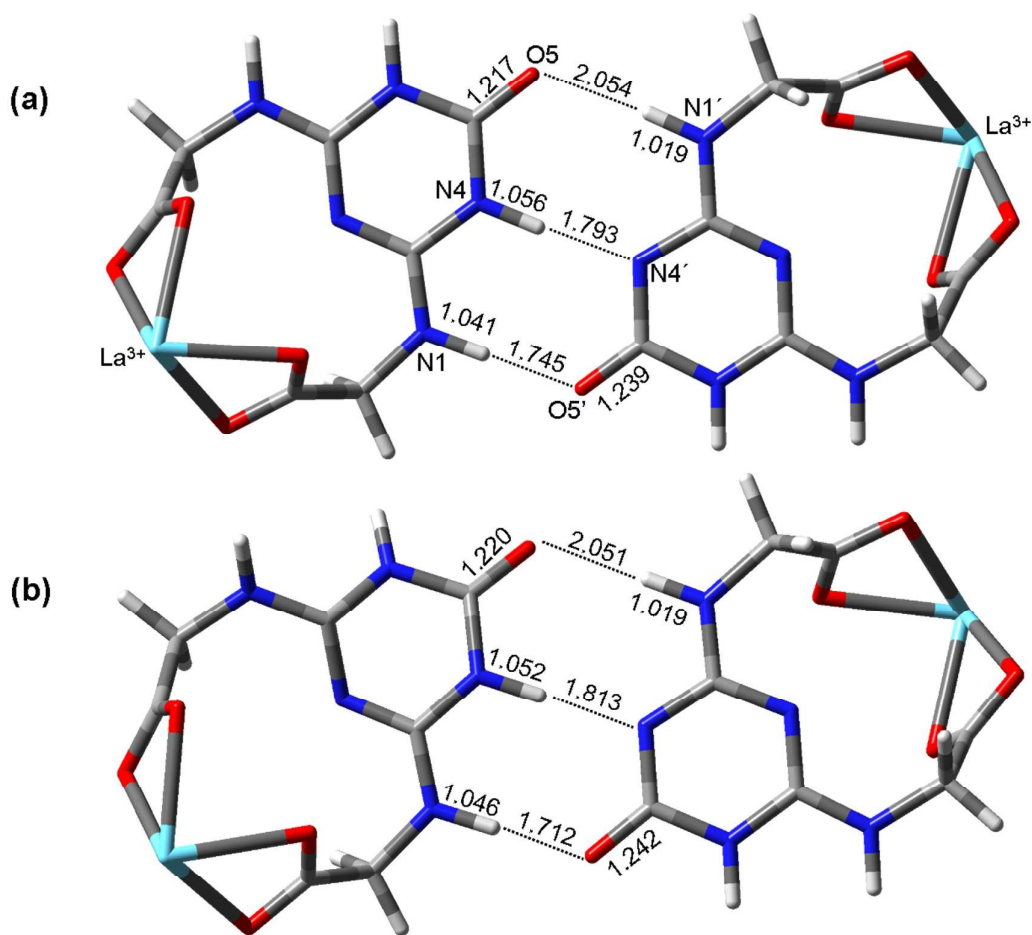
**Fig. 8** Excitation spectra of  $[(\text{La}_{0.95}\text{Eu}_{0.05})(\text{bodt})(\text{Hbodt})]$  (**2**) recorded at ambient temperature (black line) and at 12 K (red line) while monitoring the emission at 614 nm ( ${}^7\text{F}_2$  level of  $\text{Eu}^{3+}$ ). The excitation spectrum of  $[\text{La}(\text{bodt})(\text{Hbodt})]$  (**1**) (blue line) at 12 K, while detecting the emission at 420 nm, is provided for comparative purposes.

**Figure 9**

**Fig. 9** Emission spectra of  $[(La_{0.95}Eu_{0.05})(bodt)(Hbodt)]$  (2) recorded at ambient temperature (black line) and at 12 K (red line). Excitation wavelength of 394 nm.

**Figure 10**

**Fig. 10** Excitation (black lines) and emission (red lines) spectra of the [La(bodt)(Hbodt)] (1) material recorded at 295 and 12 K. The excitation was monitored at the maxima of the respective sharp emission lines, 385 and 367 nm for 295 and 12 K, respectively. The excitation wavelength was fixed at 306 nm for both emission spectra.

**Figure 11**

**Fig. 11** Optimized molecular geometries of the (a) ground-state singlet ( $S_0$ ) and (b) lowest-lying singlet excited state ( $S_1$ ) of the simplified model obtained from DFT and TD-DFT calculations, respectively. The labelling of the atoms involved in the interactions and the calculated bond lengths and intermolecular  $\text{H}\cdots\text{N}$  and  $\text{H}\cdots\text{O}$  distances (in Å) are provided for illustrative purposes.